
Article:
Navalón, G., Marugán-Lobón, J., Bright, J.A. et al. (2 more authors) (2020) The consequences of craniofacial integration for the adaptive radiations of Darwin's finches and Hawaiian honeycreepers. Nature Ecology & Evolution, 4 (2). pp. 270-278.

https://doi.org/10.1038/s41559-019-1092-y

Figure #	Figure title One sentence only	Filename This should be the name the file is saved as when it is uploaded to our system. Please include the file extension. i.e.: *Smith_ED Fig1.jpg*	Figure Legend If you are citing a reference for the first time in these legends, please include all new references in the Online Methods References section, and carry on the numbering from the main References section of the paper.
Extended Data Fig. 1	**Extended Data Figure 1 | Landmarks and semilandmarks used in this study for the beak (white) and skull (black) blocks.**	EXTENDED DATA FIGURE 1.tif	Landmark definition in Extended Data Table 1.
Extended Data Fig. 2	**Extended Data Figure 2. Landmarks used in this study.**	EXTENDED DATA FIGURE 2. LANDMARK DEFINITION.tif	
Extended Data Fig. 3	**Extended Data Figure 3 | Tempo and mode of craniofacial shape evolution in landbirds (labelled by major radiations).**	EXTENDED DATA FIGURE 3.tif	Phylomorphospaces of the first three PCs (A) and rates of evolution (B) for the whole skull configurations. Dot colours in phylomorphospaces (A) correspond to each major landbird lineage (colour legend by each silhouette in B). Branch colours in B indicate relative rate of shape evolution. Inferred rate shifts with higher posterior probability than 0.7 are plotted in corresponding branches (circles) or nodes (triangles) in the phylogeny in B. Posterior probability of each inferred rate shift is indicated by size as indicated in the legend in B.
Extended Data Fig. 4	**Extended Data Figure 4 | Tempo and mode of beak shape evolution in landbirds (labelled by major radiations).**	EXTENDED DATA FIGURE 4.tif	Phylomorphospaces of the first three PCs (A) and rates of evolution (B) for the beak block configurations. Colours and legends as before.
Extended Data Fig.	**Extended Data Figure 5 | Tempo and mode of skull shape evolution**	EXTENDED DATA FIGURE 5.tif	Phylomorphospaces of the first three PCs (A) and rates of evolution (B) for the skull block configurations.

5	**in landbirds (labelled by major radiations).**		Colours and legends as before.
Extended Data Fig. 6	**Extended Data Figure 6 | Shape differences associated with the first pair of PLS vectors (PLS1) for the beak block and the skull block for the main lineages of passerines.**	EXTENDED DATA FIGURE 6.tif	Polar histograms summarizing angle comparisons between the PLS1 vectors for the beak (B) and skull (C) blocks. As orientation of PLS1 vectors is arbitrary, the maximum possible angle between PLS1 vectors is 90°. * indicates single angular comparison of the PLS1 vectors of Passeroidea excluding DF and HH.
Extended Data Fig. 7	**Extended Data Figure 7 | Extreme morphologies and spread along lines of least resistance for each family within the parvorder Passeroidea in our sample.**	EXTENDED DATA FIGURE 7.tif	Within-family maximum Procrustes distances for PLS1scores (situation 2) for both beak and skull blocks. Done for all the families that include two or more species in our sample. Legend for labels in Extended Data Table 2. Dot colours correspond to the ages of the most common recent ancestor (MRCA) for each of the focal families in our MCC tree.
Extended Data Fig. 8	**Extended Data Figure 8 | Relationship between levels of cranial integration and evolutionary rates per clade.**	EXTENDED DATA FIGURE 8.tif	Dotplot showing the relationship between mean and median log-rate per landbird/passerine clade (clades as defined in Figures 3, 4 and Table 1) with mean clade zscore values (i.e. evolutionary covariation, situation 2). Dashed ellipses encompass the values for selected clades: 1, All landbirds; 2, Non-passerines; 3, Passeriformes; 4, Passeri; 5, Tyranni; 6, Psittaciformes; P.1, Passeroidea (including Darwin's finches and Hawaiian honeycreepers); P.2. Passeroidea (excluding Darwin's finches and Hawaiian honeycreepers).

Extended Data Fig. 9	**Extended Data Figure 9	Legend for family names**.	EXTENDED DATA FIGURE 9.tif	Figure 4c, 4d and Extended Data Figure 6.
Extended Data Fig. 10	**Extended Data Figure 10	Comparisons of the pattern of maximum covariation lines between Passeroidea and other selected passerine clades.**	EXTENDED FIGURE 10.tif	Angles (θ, degrees) for each pair of PLS1 vectors for the beak and skull block in situation 2 between Passeroidea (including and excluding DF and HH), Muscicapida (the parvorder that includes the passerine radiations sympatric to DF and HH) and Passeriformes, Passeri (all oscine passerines) and Tyranni (all suboscine passerines). As orientation of PLS1 vectors is arbitrary, the maximum possible angle between PLS1 vectors is 90°. * excluding DF and HH.

1

Item	Present?	Filename This should be the name the file is saved as when it is uploaded to our system, and should include the file extension. The extension must be .pdf	A brief, numerical description of file contents. i.e.: *Supplementary Figures 1-4, Supplementary Discussion, and Supplementary Tables 1-4.*
Supplementary Information	Yes	SI_FINAL_TEXT.pdf	Extended Results, Supplementary Figures 1-6, Supplementary Table 1-3, Supplementary References
Reporting Summary	Yes	Navalon_et_al_reporting_summary.pdf	

2

3

Type	Number If there are multiple files	Filename This should be the name the file is saved as	Legend or Descriptive

	of the same type this should be the numerical indicator. i.e. "1" for Video 1, "2" for Video 2, etc.	when it is uploaded to our system, and should include the file extension. i.e.: *Smith_ Supplementary Video 1.mov*	Caption Describe the contents of the file
Supplementary Data	Supplementary Data	SUPPLEMENTARY_DATA_ALL.xlsx	Supplementary Data Tables 1-5

Title: The consequences of craniofacial integration on the adaptive radiations of Darwin's Finches and Hawaiian Honeycreepers

Guillermo Navalón[1,2,3*], Jesús Marugán-Lobón[2,4], Jen A. Bright[5,6], Christopher R. Cooney[7] & Emily J. Rayfield[1,*]

1. School of Earth Sciences, University of Bristol, Life Sciences Building, Bristol, UK

2. Unidad de Paleontología, Departamento de Biología, Universidad Autónoma de Madrid, Madrid, Spain

3. Department of Earth Sciences, University of Oxford, Oxford OX1 3AN, United Kingdom.

4. Dinosaur Institute, Natural History Museum of Los Angeles County, Los Angeles, CA, USA.

5. School of Geosciences, University of South Florida, Tampa, FL 33620, USA

6. Department of Biological and Marine Sciences, University of Hull, Hull HU6 7RX, UK7.Department of Animal and Plant Sciences, University of Sheffield, Sheffield S10 2TN, UK.

*Corresponding authors. E-mails: gn13871@bristol.ac.uk, e.rayfield@bristol.ac.uk

The diversification of Darwin's finches and Hawaiian honeycreepers are two textbook examples of adaptive radiation in birds. Why these two bird groups radiated while the remaining endemic birds in these two archipelagos exhibit relatively low diversity and disparity remains unexplained. Ecological factors have failed to provide a convincing answer to this phenomenon, and some intrinsic causes connected to craniofacial evolution have been hypothesized. Tight coevolution of the beak and the remainder of the skull in diurnal raptors and parrots suggests that integration may be the prevalent condition in landbirds (Inopinaves). This is in contrast with the archetypal relationship between beak shape and ecology in Darwin's finches and Hawaiian honeycreepers, which suggests the beak can adapt as a distinct module in these birds. Modularity has therefore been proposed to underpin the adaptive radiation of these birds, allowing the beak to evolve more rapidly and 'freely' in response to ecological opportunity. Here, using geometric morphometrics and phylogenetic comparative methods in a broad sample of skulls of landbirds, we show that craniofacial evolution in Darwin's finches and Hawaiian honeycreepers appears to be characterized by a tighter coevolution of the beak and the rest of the skull (cranial integration) than in most landbird lineages, with rapid and extreme morphological evolution of both skull regions along constrained directions of phenotypic space. These patterns are unique among landbirds, including other sympatric island radiations, and therefore counter previous hypotheses by

showing that tighter cranial integration, not only modularity, can facilitate evolution along adaptive directions.

Why some lineages diversify more or less than others is a central topic in evolutionary biology. Among birds, the adaptive island radiations of Darwin's finches and Hawaiian honeycreepers are notable for their rapid and disparate evolution[1,2]. These clades quickly evolved to become taxonomically and morphologically more diverse than other avian lineages that colonized the same oceanic archipelagos[3-7]. Since these phenomena were first recognized[8,9], many different causal hypotheses have been proposed to explain such rapid island radiations. Extrinsic causes, such as differences in colonization age, have been largely dismissed because other slower evolving lineages of birds colonized the archipelagos at similar times[3-5,10]. Alternatively, intrinsic explanations may offer more insight[4,5,11,12]. *In silico* simulations and empirical studies show that the covariation structure of sets of characters (produced by genetic, developmental, functional, or evolutionary causes) have important influences in phenotypic evolution (Fig.1) (e.g.,[13-15]). For example, simulations show that if an anatomical structure is integrated (its component parts co-evolve, *sensu*[16]), its phenotypic evolution will be constrained along specific lines within trait space. Modularity (weaker integration between component parts), in turn, allows a less constrained exploration of trait space[13,17](Fig. 1a). Therefore, a more modular organization is traditionally believed to facilitate, or even to be a precondition[18] for evolvability[19] by allowing component parts to evolve and adapt more independently from each other[20,21]. An alternative view is that integration may enhance evolvability, by providing an adaptive line of least resistance, along which species may rapidly evolve, albeit within a constrained region of trait space [13,17,22-24] (Fig. 1c). Although the degree to which integration and modularity affect evolution seems to be controlled by selection, some empirical discrepancies still exist[13,17,22-24].It might be expected that birds, a speciose vertebrate group with extremely divergent beak shapes, demonstrate little covariation between the beak and the remainder of the skull. At a broad macroevolutionary level this holds true and the beak evolved as a semi-independent structure displaying weak integration with the rest of the skull, arguably explaining its evolutionary plasticity[25]. Yet, when integration is quantified at the family/subfamily level, studies have shown strong integration between the beak and skull morphology in diurnal raptors and parrots[11,26]. Raptors and parrots occupy key phylogenetic positions at the base and within the landbird (Inopinaves) radiation, respectively[27-29](which also includes Darwin's finches and Hawaiian honeycreepers) suggesting that strong cranial integration might be ancestral to and prevalent in landbirds[11,26]. While there is no inherent reason to preclude that selection on the shape of the beak would not also lead to adaptive changes in the shape of cranium, strong cranial integration within these clades has been suggested to reflect pleiotropic interactions among cranial regions hampering a fine adaptation of beak shape to feeding ecology[11,26]. This is in contrast to the paradigmatic relationship between feeding ecology and beak size and shape evolution in Darwin's finches [30,31] and Hawaiian honeycreepers [5,32] which suggests the beak in these clades is able to respond effectively and more or less independently to feeding selective pressures in their island ecosystems (an observation that was crucial to developing the theory of natural selection[8,33]). A key question therefore is whether relaxation of cranial integration represents an evolutionary innovation in these landbird clades whereby the beak is

able to evolve more 'freely', thereby facilitating rapid evolutionary radiation[11,12], or if integration facilitates rapid evolution along constrained adaptive directions. The recent surge of interest in the implications of integration and modularity for evolvability in evolutionary theory [11,13,15,25,34] makes testing these ideas in an iconic example of adaptive radiation particularly relevant. Therefore, using geometric morphometrics and phylogenetic comparative methods we here quantify whether relaxed integration (modularity) between the beak and skull is linked to rapid and disparate evolutionary radiation in landbirds as per classic interpretations, or whether tighter integration may be key to rapid and large evolutionary change.

Results & Discussion

We found that each of the major clades of landbirds diverged to unique cranial morphologies (Fig. 2, Extended Data. Figs. 3-5). Parrots (Psittaciformes) are characterised by a single ancestral shift towards very high rates of skull shape evolution, resulting in a characteristic cranial anatomy with short, curved beaks and expanded braincases (Fig. 2). Conversely, hoopoes and hornbills (Bucerotiformes) and toucans (Ramphastidae, Piciformes) show similar skull shapes to parrots but have higher aspect ratio, less curved beaks (Extended Data. Figs. 3-5). While passerines (Passeriformes) have radiated to explore a large proportion of landbird morphological variation, they have not achieved the levels of morphological variation seen in non-passerines (Fig. 2). Although most passerines display similar skull morphologies and there is a slowdown in rates of skull shape evolution in the branch leading to the songbirds (Passeri), a few songbird lineages diverge substantially to explore morphologies approaching those of parrots or hoopoes (Fig. 2, Extended Data. 3-5). Darwin's finches and Hawaiian honeycreepers show the highest rates of beak and skull shape evolution in our sample, and experienced multiple positive rate shifts within each clade. This result is similar to that of other recent studies[2,25], suggesting that the rapidity of evolution in these species is not simply a result of their relatively recent divergence relative to the other species in our data. These birds also show considerable craniofacial shape disparity, including some of the most extreme shapes within Passeriformes (Fig. 2).

We found that the beak and the skull are integrated to an extent in all landbird clades (Fig. 3a, Fig. 4a). When considered as separate groups, Passeriformes have more integrated skulls than non-passerines (Fig. 4a, Table 1). This is driven by high integration in the songbirds (Passeri), moderately high integration in the suboscine passerines (Tyranni) within the Passeriformes, and high integration in the parrots (Psittaciformes) within the non-passerines (Fig. 3a, Fig. 4a, Table 1, Extended Data Fig. 10). All other clades show lower and similar levels of cranial integration (Fig. 3a, 4a; Table 1). Within songbirds (Fig. 4b), Passerida, the clade containing Darwin's finches and Hawaiian honeycreepers, exhibits higher levels of integration than all other passerine clades and this likely underscores the high integration displayed by songbirds as a whole group. Interestingly, the Muscicapida, the other passerine clade that radiated in Galapagos and Hawaii (but to a lesser extent than Darwin's finches and Hawaiian honeycreepers), display the lowest levels of integration in our sample (Fig. 3b, 4b, Table 1). High levels of integration and the same pattern of covariation persist in Passerida even when Darwin's finches and Hawaiian honeycreepers are removed from the

analysis (Fig. 3b, 4b; for congruence of these results with other analytical conditions see SI. Figs. 5 & 6, Extended Data Fig. 10, Supplementary Data 1 & 2), suggesting that craniofacial covariation in these clades matches the general covariation pattern of Passerida, indicating high cranial integration may be more widespread in this clade. Therefore, contrary to previous suggestions, our results show that cranial evolution in the classic adaptive radiations of Darwin's finches and Hawaiian honeycreepers was most likely characterised by a pattern of strong integration between of the beak with the rest of the skull.

Although there is not a common relationship between the strength of cranial integration and rates of morphological evolution for all landbirds in our data (Extended Data Fig. 8), this matches expectations as recent *in silico* models and empirical data show that this relationship is also critically dependent on selection impinging upon functional and developmental factors [15,17,23,24,35]. Specifically, evolution along phenotypic lines of least resistance[23] predicts that, by affecting several traits in unison, higher trait covariation can increase evolutionary rates if selection favours evolutionary change along the line of maximum covariation[17,23,24], allowing more extreme morphologies to be explored [13,36]. Therefore, lack of correlation in an older lineage such as parrots (~ 30 MY crown-group Psittaciformes,[29]) may be due to clade age: this lineage has been affected by multidirectional selective pressures during its long evolution, complicating the identification of a straightforward relationship between strong evolutionary integration of the skull and phenotypic evolution (i.e., the 'fly in a tube' model[15]). Conversely, Darwin's finches and Hawaiian honeycreepers (and sympatric contemporaneous radiations) are much younger clades (Fig. 4c), and geographically restricted to their islands, and therefore represent a rare opportunity to make more detailed inferences of phenotypic evolution. Relaxed selection in island ecosystems is often invoked as resulting from the availability of empty niche space and scarcity of predators, particularly in newly colonized islands (i.e. 'the island rule' [37,38]). Although this selection regime is often linked to divergent evolution[37], it may also facilitate evolution along lines of least resistance by raising the probability of selection favouring change along adaptive phenotypic pathways. Although adaptive peaks could potentially arise in more areas of trait space if selection is more flexible (therefore allowing more directions of evolution), the most likely change will by definition be the one using the line of least resistance (Fig. 1). For example, evolution along an allometric line of least resistance rather than divergent evolution may have facilitated the repeated evolution of phyletic dwarfism in island elephants[39]. In a similar way, the constrained evolution of extreme morphologies along the maximum covariation line in Darwin's finches and Hawaiian honeycreepers might have favoured both rapid allopatric speciation and rapid niche separation by character displacement within each of the families because selection facilitating change in one cranial trait affected a cascade of other cranial regions[37]. This, in turn, might underlie the comparatively higher rates of morphological evolution for the whole skull, and for both the beak and skull individually (Fig. 2 & SI. Tables 1-3; and see also [2,25]). In agreement with this model, we show that at the family level (or sub-family for Darwin's finches and Hawaiian honeycreepers), Darwin's finches and Hawaiian honeycreepers exhibit some of the most extreme shape differences along the axis of maximum covariation between the beak and the skull shapes (the purported phenotypic line of least resistance; see Methods) for the

passeroid songbirds (Passerida) (Extended Data. Fig. 7) and for all songbirds (Fig 4c). This coordinated phenotypic evolution (Extended Data. Fig. 6) might also be biomechanically significant, as the jaw adductor muscles attach exclusively to the braincase block, yet act to power the beak during forceful biting. Increased integration between the beak and braincase may therefore facilitate improved feeding performance in both the beak and the rest of the skull in Hawaiian honeycreepers and in Darwin's finches, for whom a demonstrated link between beak morphology and feeding exists[40]. This directional evolution may also have produced some of the highest values of total craniofacial disparity at the family/subfamily level for both clades (Fig. 4b), which is particularly striking considering that Darwin's finches and Hawaiian honeycreepers are substantially younger than most of the other considered families (Fig.4c). Therefore, the constrained (Figs. 3, 4b & 4d, Table 1, Extended Data. Fig. 7), but morphologically extreme (Figs. 2 & 4c) and rapid (Fig. 2), craniofacial evolution in Darwin finches and Hawaiian honeycreepers meets the expectations of rapid evolution along lines of phenotypic least resistance[17,23], where high integration, rather than high modularity, facilitates evolution along a particular adaptive morphocline.

Rapid evolution along lines of phenotypic least resistance may also explain the apparent contradiction between large phenotypic divergence despite little change in genetic divergence between species in Darwin's finches and in Hawaiian honeycreepers [3,5]. It may also shed some light on why other passerine lineages that colonized both archipelagos at similar times failed to undergo the same explosive adaptive radiation. In Hawaii, the two endemic lineages of passerine birds that colonized the archipelago at similar times to Hawaiian honeycreepers are the Hawaiian thrushes (5 species, Turdidae)[5], and the extinct Hawaiian honeyeaters (5 species, Mohoidae)[10]. Both families belong to the parvorder Muscicapida, the passerine lineage exhibiting the lowest integration in our data (Fig. 4a). Similarly, the other endemic radiation in the Galapagos archipelago, the Galapagos mockingbirds (4 species, Mimidae, also in the Muscicapida), colonised the islands at a similar time but did not undergo a rapid diversification[4]. While multiple ecologically relevant traits of the colonizer species may have contributed to the diversification patterns of passerines in Galapagos and Hawaii, we suggest that their lower craniofacial integration may have been an important factor preventing them exploiting adaptive lines of least resistance that likely produced the rapid and large evolutionary change in cranial morphology that we showed in Darwin's finches and Hawaiian honeycreepers. Nonetheless, our study demonstrates that adaptive radiations are possible under tighter cranial integration.

In summary, we propose that a stronger craniofacial integration was a key factor shaping the extreme craniofacial evolution of two classic radiations of island passeroids. While an intrinsic evolutionary lability of the beak has been proposed for several families of passeroid songbirds [5,31,32,40], other studies have shown that beak shape among the group is constrained to a small series of shape transformations arising from a constrained morphogenetic program[41]. Our hypothesis reconciles both views by showing that although high cranial integration constrains the shapes of the beak and skull, it may also facilitate evolutionary lability along specific phenotypic clines in particular ecological scenarios.

Acknowledgements

We are thankful to Joanne Cooper and Judith White (NHM Tring), and Christopher M. Milensky and Brian K. Schmidt (Smithsonian National Museum of Natural History) for access to specimens. We thank Fernando Blanco, Matteo Fabbri, Iris Menéndez, and Luis Porras for enlightening discussion on the evolutionary implications of this research. We are grateful to Gavin Thomas, Thomas Püschel, Chris Klingenberg, Armin Elsler, Frane Babarović and Soledad de Esteban-Trivigno for enlightening insights and discussion on the methods. We thank Óscar Sanisidro and Lucía Balsa Pascual for design and technical advice that greatly improved the quality of the graphic support. GN was supported by a PG Scholarship/Studentship from The Alumni Foundation, University of Bristol, UK and is currently supported by the ERC project 'TEMPO' (grant number: 639791). JML is supported by the Spanish MINECO, Project CGL-2013-42643. EJR and JAB were supported by a BBSRC grant BB/I011668/1.

Author's contributions

The focus and design of this research was developed by GN, JM-L, JAB and ERJ. CRC conducted the Variable Rates Model Analyses. GN conducted the remaining of the analyses. GN JM-L, JAB, CRC and ERJ co-wrote the manuscript.

Competing interests

The authors declare no competing financial interests.

METHODS

Database and phylogenetic hypothesis

Our study includes 128 families of landbirds (i.e: Inopinaves, defined as Telluraves (Yuri et al. 2013) + *Opisthocomus hoazin*, Prum et al. 2015) giving a total of 436 species (Supplementary Data 5. List of specimens). All but five families within the landbird radiation are represented in our sample (Philepittidae, Sapayoaidae, Dasyornithidae, Urocynchramidae and Aegithinidae). These families are either monotypic or have an extremely reduced diversity, and often regarded as belonging within other passerine families [44]. Sampling was non-random and aimed to capture the maximum beak morphological disparity within each family, with a special focus on the subfamilies of Darwin's finches (Geospizinae) and Hawaiian honeycreepers (Drepanidinae) (represented in our sample by ~70% and ~ 60 % of their extant diversity, respectively). A time-calibrated maximum clade credibility (MCC) phylogeny of the 436 species was generated using TreeAnnotator[45] from a population of 10,000 'Hackett's backbone stage 2 trees'. Trees were generated using the in-built tools from www.birdtree.org (for full details regarding tree construction methods, see[1]), and branch lengths were set equal to 'Common ancestor' node heights. The resulting MCC phylogeny is largely congruent with the last genomic phylogenies for the interrelationships of landbirds (Figs. 2, 4a & 4b,[28,29]).

Geometric morphometrics

A set of 17 landmarks and 2 curves (three evenly separated semilandmarks along the dorsal and ventral rims of the beak) was digitized using the software tpsDig.2[46] in lateral views of the skull of each specimen (Extended Data Fig. 1, Landmark position/ Extended Data. Fig. 2, Landmark definition). The Minimum Bending Energy criterion was applied to slide the semilandmarks in tpsRelw[47], as this is more appropriate than the Minimum Procrustes Distance criterion when dealing with data with high morphological variation in the software used here[48]. Landmarks and semilandmarks were then classified as belonging to the 'beak block' (block 1) or 'skull block' (block 2) (Extended Data Figs. 1 & 2). Shape data (Procrustes coordinates) was extracted using three different full Generalized Procrustes Analyses (GPAs) for: 1) the whole landmark configuration; 2) the 'beak block'; and 3) the 'skull block'. An additional Generalized Resistant Procrustes Superimposition (GRPS,[49]) was conducted in the raw coordinates from the whole landmark configuration to identify possible trait-correlation artefacts in our shape data (see Methods. Evolutionary covariation & SI). GPA aligned Procrustes coordinates were thereafter imported to MorphoJ[50] and the R statistical environment[51] for all downstream analyses.

Principal Component Analyses (PCA) and Variable Rates Model Analyses (VRMA)

To explore the main patterns of skull shape variation in landbirds, we conducted Principal Component Analyses (PCAs) for: 1) the whole configuration; 2) the 'beak block'; and 3) the 'skull block'. The time-calibrated MCC phylogeny was mapped over the PCAs by weighted (i.e., including branch length information) square-change parsimony in order to visualize evolutionary changes over the morphospace. Principal Components Analyses (including mapping time calibrated trees) were conducted in MorphoJ.

To explore the tempo of craniofacial evolution in landbirds, we used the scores derived from the previous PCAs to conduct Variable Rates Model Analyses (VRMAs) using the software BayesTraits V2.0.2[52] (available from http://www.evolution.rdg.ac.uk/). This method uses a reversible jump Markov chain Monte Carlo (MCMC) approach to estimate the location, probability, and magnitude of rate shifts in continuous traits across branches of a phylogenetic tree (see[53]). We used PC scores for: 1) the whole skull (13 PCs); 2) the 'beak block' (6 PCs); and 3) the 'skull block' (10 PCs). We used the number of principal components that account for 95% of shape variance, except for the whole configuration where we used the number that account for 90% to avoid poor performance due to a high number of variables[54]. We ran two replicate chains for each model using default priors and assuming uncorrelated trait axes[2]. Each chain was run for 200,000,000 iterations (sampled every 10,000 iterations), with the first 100,000,000 iterations removed as burn in. We confirmed that replicate runs had converged and combined the output of both runs for further analysis. We summarized the results of each run by calculating (1) the mean rate, and (2) the probability of a rate shift (branch or clade) over all posterior samples for each node in the tree. In the main text, we focus on rate shifts that are inferred with higher posterior probability (PP) than 0.70. To account for rate heterogeneity in downstream analyses of evolutionary covariation (see Methods. Evolutionary covariation and SI), a rate-scaled phylogeny (non-ultrametric) was generated by using the branch lengths predicted by the model of the VRMA conducted with the whole skull configurations.

Evolutionary covariation

Evolutionary covariation between the 'beak block' (block 1) and the 'skull block' (block 2) was examined for each of the clades of landbirds by means of Phylogenetic Partial Least Squares analysis (P-PLS,[55,56]) in three different situations: two blocks using the calibrated time tree (separate GPA for the 'beak block' and the 'skull block') (situation 1); two blocks using the rate-scaled phylogeny (situation 2); and within one configuration (one single GPA for the whole configuration) using the rate-scaled tree (situation 3). Phylogenetic Partial Least Squares (P-PLS) is a multivariate analysis that quantifies the evolutionary covariation between two different sets of data by searching for vectors of correlated variables without implying predictability of one set of variables upon the other.

Although least-squares GPA[57] provides a universal criterion for defining shape data, and convenient statistical properties for downstream multivariate analyses that other superimposition methods do not[58], it has some widely recognised limitations when shape differences between landmarks are highly heterogeneous [49,59-61]. This is because GPA assumes that variation among landmarks is homogeneous and that all landmarks vary isotropically[57] (they are equally distributed in all directions). Therefore, if a great deal of the total shape difference is concentrated in just a few landmarks, and/or its variation is skewed towards one or more directions, GPA tends to spread this localized shape variance across the whole configuration, generating artefactual shape differences[49,61-63](i.e., the 'Pinocchio effect'[62]). This issue can be particularly misleading when evaluating covariation patterns (i.e. integration and modularity) as it tends to overestimate integration. There is still debate as to whether this is a critical concern in real biological data or not[49,61,64], however, in an exploratory study Cardini[61], showed that GPA can generate artefactual patterns of covariation even if the original shape data exhibits no covariation at all. The fact that landbirds demonstrate high beak shape variation relative to other skull regions[25,34] led us to contemplate this possibility. Therefore, to identify whether the aforementioned might be a problem in our sample, we carried out a Generalized Resistant Procrustes Superimposition (GRPS[49,60]) in the raw coordinates (unaligned) for the whole configurations for all landbirds and compared them with a GPA superimposition using Resistant Procrustes Software (RPS[49], available online at: https://sites.google.com/site/resistantprocrustes/) (SI. 4). GPRS differs from GPA in that the set of criteria for eliminating rotational information from shape data are estimated through a repeated-medians calculation for each dataset, rather than minimizing the squared sum of Euclidean distances between the landmark coordinates[60]. This criterion is therefore robust to larger variation in a few landmarks with respect to the whole configuration, and thus better portrays localized variation across coordinates[49,60]. Additionally, we tested evolutionary shape covariation between blocks 1 and 2 within one configuration (situation 3, single GPA) to gain insight on how localized variation might affect integration results in our sample (SI. Expanded Results, SI. Figs. 5 & 6; SI. Table 2).

Because GPRS and other resistant-based procedures are not based in Procrustes distances, concerns have been expressed regarding their ability to generate shape tangent spaces appropriate for Euclidean multivariate statistics (e.g.,[65]). Although there are specifically implemented multivariate methods for dealing with data extracted from a GPRS,

the standard usage of GPA in modern geometric morphometrics[66,67] means that most available methods are based on Procrustes distances. These Procrustes-based analyses need the consistency with the Procrustes projection that defines shape variables in geometric morphometrics[58]. To our knowledge, there is not currently an appropriate method able to overcome both trait correlation artefacts yet retain an equivalence with Euclidean multivariate statistics. Consequently, we are forced to quantify covariation using two blocks (situations 1 and 2) in an attempt to mitigate any artefactual spread of variance across the whole configuration (see SI. Expanded Results for further details). This approach is better at portraying the original patterns of local variation in geometric morphometrics and generally eliminate artefactual trait covariation, at least as far as integration is concerned[61]. However, covariation in situations 1 and 2 only reflects evolutionary shape covariation, as information regarding relative size and arrangement between blocks is lost (eliminated in each block's separate GPA) and can only be accessed indirectly (e.g., because the shape data is a 2-dimensional projection of a 3D object, certain shape changes might be indicative of differences in arrangement angle).

Several studies have shown that landbirds exhibit extreme heterogeneity of rates of craniofacial evolution [2,25], which we also quantified here (Fig 2; SI. Tables 1-3). Computation of Phylogenetic Partial Least Squares in *geomorph*[68] assumes a single-rate Brownian Motion model of evolution which is unlikely to conform to shape data that evolved with highly heterogeneous rates. When shape data does not conform to a single-rate BM model, previous approaches rescaled the branch lengths of the phylogeny using the parameters estimated by the model that best fits the data from a selection of *a priori* models, namely: single-rate BM, Ornstein–Uhlenbeck, and Early-Burst (e.g,[69]). This approach coerces the phylogenetic covariation matrix to approximate a BM model, therefore meeting the expectations of the analysis. However, recent research has shown that current model-fitting methods based on maximum-likelihood tend to exhibit ill-conditioned covariation matrices, leading to misidentifications of the model of evolution[54], even when the data is generated under a particular model like BM [70]. Here, we chose a different approach: we used the branch lengths estimated by the VRMA for the whole skull configuration. In this way, we rescaled the branch lengths in our tree to account for the actual rates of phenotypic evolution rather than using parameters estimated by the fit to a particular set of *a priori* single-process models. Although this solution is not ideal, it allows for the inclusion of branch lengths estimated by more complex models than previous approaches, which have also been shown to exhibit best fits for other cases of trait evolution like body mass[71]. The methodological endeavour needed to implement more complex evolutionary models in phylogenetic comparative methods for high dimensional data[72] goes well beyond the scope of this study. Here, comparisons between situations 1 (two blocks using the calibrated time tree) and 2 (two blocks using the rate-scaled tree) aimed to gain insight on the effects of accounting for variable rates in evolutionary covariation in measures of evolutionary integration (SI. Figs. 2 & 3; Supplementary Data 3).

The strength of evolutionary covariation in each of the three scenarios was compared and tested between major radiations of landbirds and between the major radiations of passerines following a recently developed statistical procedure[73]. The major non-passerine

radiations were compared to the major subdivisions of the Passeriformes (Passeri and Tyranni) based on the high support in all the latest phylogenetic hypotheses of these clades and similar node age estimations[29]. The more recently-branching passerine parvorders were compared between each other. As P-PLS correlation values (*rpls*) have been shown to be influenced by sample size[74], comparing or testing for differences in integration levels between two different sample sizes using this statistic is problematic. Adams & Collyer[73] recently proposed the use of *rpls* effects sizes (z-scores). Z-scores were therefore calculated as the standard deviates of the *rpls* values from the permutation procedure for the P-PLS analyses of each clade, and confidence intervals were calculated for each value. Pairwise differences in z-scores were then compared and statistically tested in order to discriminate between levels of integration between clades. Z-score values were used directly to elucidate which clades exhibited higher integration when differences were found. To explore the differences in the pattern of cranial integration between clades, pairwise angles and correlations of PLS1 vectors (the pair of vectors that covary most for each P-PLS) were calculated for all the clades in situation 2 (Extended Data Fig. 6; Extended Data Fig. 10; SI. Fig. 1; Supplementary Data 1 & 2). Histograms of frequency of binned angles and shape differences across each vector were plotted for visual comparisons (Extended Data Fig. 6; SI. Fig. 1).

Finally, we addressed whether stronger cranial integration generated greater morphological change along the evolutionary line of least resistance in Darwin's finches and Hawaiian honeycreepers than in other landbird families. To do so, we computed maximum distances within each family (or subfamily for Geospizinae and Drepanidinae) of landbirds for the PLS1 scores of the beak and skull blocks as a proxy of the degree of spread along the line of least resistance. We did this for the PLS1 axes defined for each order (and Passeri and Tyranni for the Passeriformes) and compared PLS1 distances for the beak and skull block between all the families. Furthermore, we repeated this for the parvorder Passerida and compared PLS1 distances for the beak and skull block between passeroid families alone. To ascertain whether a larger spread across the lines of least resistance also corresponds to more extreme cranial morphologies, we computed maximum Procrustes distances within each family/subfamily using the Procrustes coordinates (both from the whole configuration and beak and skull blocks separately).

Data availability

All relevant data is available via the University of Bristol's DataBris repository at https://data.bris.ac.uk/data/dataset/3kpwgpnqewcy2tvak6uzzdztt.

Literature

1 Jetz, W., Thomas, G., Joy, J., Hartmann, K. & Mooers, A. The global diversity of birds in space and time. *Nature* **491**, 444-448 (2012).

2 Cooney, C. R. *et al.* Mega-evolutionary dynamics of the adaptive radiation of birds. *Nature* **542**, 344-347 (2017).

3 Burns, K. J., Hackett, S. J. & Klein, N. K. Phylogenetic relationships and morphological diversity in Darwin's finches and their relatives. *Evolution* **56**, 1240-1252 (2002).

4 Arbogast, B. S. *et al.* The origin and diversification of Galapagos mockingbirds. *Evolution* **60**, 370-382 (2006).

5 Lovette, I. J., Bermingham, E. & Ricklefs, R. E. Clade-specific morphological diversification and adaptive radiation in Hawaiian songbirds. *Proceedings of the Royal Society of London B: Biological Sciences* **269**, 37-42 (2002).

6 Pratt, H. D. & Conant, S. *The Hawaiian Honeycreepers: Drepanidinae*. (Oxford University Press, 2005).

7 Tokita, M., Yano, W., James, H. F. & Abzhanov, A. Cranial shape evolution in adaptive radiations of birds: comparative morphometrics of Darwin's finches and Hawaiian honeycreepers. *Phil. Trans. R. Soc. B* **372**, 20150481 (2017).

8 Darwin, C. *The Zoology of the Voyage of HMS Beagle: Under the Command of Captain Fitzroy, RN, During the Years 1832 to 1836: Published with the Approval of the Lords Commissioners of Her Majesty's Treasury*. (Smith, Elder and Company, 1839).

9 Mayr, E. The zoogeographic position of the Hawaiian Islands. *The Condor* **45**, 45-48 (1943).

10 Fleischer, R. C., James, H. F. & Olson, S. L. Convergent evolution of Hawaiian and Australo-Pacific honeyeaters from distant songbird ancestors. *Current Biology* **18**, 1927-1931 (2008).

11 Bright, J. A., Marugán-Lobón, J., Cobb, S. N. & Rayfield, E. J. The shapes of bird beaks are highly controlled by nondietary factors. *Proceedings of the National Academy of Sciences*, 201602683 (2016).

12 Abzhanov, A. The old and new faces of morphology: the legacy of D'Arcy Thompson's 'theory of transformations' and 'laws of growth'. *Development* **144**, 4284-4297 (2017).

13 Goswami, A., Smaers, J., Soligo, C. & Polly, P. The macroevolutionary consequences of phenotypic integration: from development to deep time. *Philosophical Transactions of the Royal Society of London B: Biological Sciences* **369**, 20130254 (2014).

14 Klingenberg, C. P. Studying morphological integration and modularity at multiple levels: concepts and analysis. *Philosophical Transactions of the Royal Society of London B: Biological Sciences* **369**, 20130249 (2014).

15 Felice, R. N., Randau, M. & Goswami, A. A fly in a tube: Macroevolutionary expectations for integrated phenotypes. *Evolution* **72**, 2580-2594 (2018).

16 Olson, E. C. & Miller, R. L. *Morphological integration*. (University of Chicago Press, 1999).

17 Villmoare, B. Morphological integration, evolutionary constraints, and extinction: a computer simulation-based study. *Evolutionary Biology* **40**, 76-83 (2013).

18 Fisher, R. A. *The genetic theory of natural selection*. (Dover, 1958).

19 Kirschner, M. & Gerhart, J. Evolvability. *Proceedings of the National Academy of Sciences* **95**, 8420-8427 (1998).

20 Wagner, G. P. & Altenberg, L. Perspective: complex adaptations and the evolution of evolvability. *Evolution* **50**, 967-976 (1996).

21 Raff, R. A. *The shape of life: genes, development, and the evolution of animal form*. (University of Chicago Press, 2012).

22 Wagner, G. Coevolution of functionally constrained characters: prerequisites for adaptive versatility. *BioSystems* **17**, 51-55 (1984).

23 Marroig, G. & Cheverud, J. M. Size as a line of least evolutionary resistance: diet and adaptive morphological radiation in New World monkeys. *Evolution* **59**, 1128-1142 (2005).

24 Hansen, T. F. Is modularity necessary for evolvability?: Remarks on the relationship between pleiotropy and evolvability. *Biosystems* **69**, 83-94 (2003).

25 Felice, R. N. & Goswami, A. Developmental origins of mosaic evolution in the avian cranium. *Proceedings of the National Academy of Sciences*, 201716437 (2018).

26 Bright, J. A., Marugán-Lobón, J., Rayfield, E. J. & Cobb, S. N. The multifactorial nature of beak and skull shape evolution in parrots and cockatoos (Psittaciformes). *BMC evolutionary biology* **19**, 104 (2019).

27 Hackett, S. J. *et al.* A phylogenomic study of birds reveals their evolutionary history. *science* **320**, 1763-1768 (2008).

28 Jarvis, E. D. *et al.* Whole-genome analyses resolve early branches in the tree of life of modern birds. *Science* **346**, 1320-1331 (2014).

29 Prum, R. O. *et al.* A comprehensive phylogeny of birds (Aves) using targeted next-generation DNA sequencing. *Nature* (2015).

30 Gibbs, H. L. & Grant, P. R. Oscillating selection on Darwin's finches. (1987).

31 Grant, P. R. & Grant, B. R. Evolution of character displacement in Darwin's finches. *science* **313**, 224-226 (2006).

32 Smith, T. B., Freed, L. A., Lepson, J. K. & Carothers, J. H. Evolutionary consequences of extinctions in populations of a Hawaiian honeycreeper. *Conservation Biology* **9**, 107-113 (1995).

33 Darwin, C. & Wallace, A. On the tendency of species to form varieties; and on the perpetuation of varieties and species by natural means of selection. *Zoological Journal of the Linnean Society* **3**, 45-62 (1858).

34 Klingenberg, C. P. Cranial integration and modularity: insights into evolution and development from morphometric data. *Hystrix, the Italian Journal of Mammalogy* **24**, 43-58 (2013).

35 Schluter, D. Adaptive radiation along genetic lines of least resistance. *Evolution* **50**, 1766-1774 (1996).

36 Randau, M. & Goswami, A. Unravelling intravertebral integration, modularity and disparity in Felidae (Mammalia). *Evolution & development* **19**, 85-95 (2017).

37 Losos, J. B. & Ricklefs, R. E. Adaptation and diversification on islands. *Nature* **457**, 830 (2009).

38 Wright, N. A., Steadman, D. W. & Witt, C. C. Predictable evolution toward flightlessness in volant island birds. *Proceedings of the National Academy of Sciences*, 201522931 (2016).

39 van der Geer, A. A., Lyras, G. A., Mitteroecker, P. & MacPhee, R. D. From Jumbo to Dumbo: Cranial Shape Changes in Elephants and Hippos During Phyletic Dwarfing. *Evolutionary Biology*, 1-15 (2018).

40 Grant, B. R. & Grant, P. R. Evolution of Darwin's finches caused by a rare climatic event. *Proceedings of the Royal Society of London B: Biological Sciences* **251**, 111-117 (1993).

41 Fritz, J. A. *et al.* Shared developmental programme strongly constrains beak shape diversity in songbirds. *Nature communications* **5** (2014).

42 Marroig, G., Shirai, L. T., Porto, A., de Oliveira, F. B. & De Conto, V. The evolution of modularity in the mammalian skull II: evolutionary consequences. *Evolutionary Biology* **36**, 136-148 (2009).

43 Renaud, S., Auffray, J. C. & Michaux, J. Conserved phenotypic variation patterns, evolution along lines of least resistance, and departure due to selection in fossil rodents. *Evolution* **60**, 1701-1717 (2006).

44 Del Hoyo, J. *et al.* Handbook of the Birds of the World Alive. Lynx Editions, Barcelona. (2017).

45 Rambaut, A. & Drummond, A. TreeAnnotator v1. 7.0. *Available as part of the BEAST package at http://beast. bio. ed. ac. uk* (2013).

46 Rohlf, F. tpsDig, version 2.10. *Department of Ecology and Evolution, State University of New York, Stony Brook* (2006).

47 Rohlf, F. tpsRelw, relative warps analysis. *Department of Ecology and Evolution, State University of New York at Stony Brook, Stony Brook, NY* (2010).

48 Perez, S. I., Bernal, V. & Gonzalez, P. N. Differences between sliding semi-landmark methods in geometric morphometrics, with an application to human craniofacial and dental variation. *Journal of anatomy* **208**, 769-784 (2006).

49 Torcida, S., Perez, S. I. & Gonzalez, P. N. An integrated approach for landmark-based resistant shape analysis in 3D. *Evolutionary Biology* **41**, 351-366 (2014).

50 Klingenberg, C. MorphoJ. *Faculty of Life Sciences, University of Manchester* **3**, 75-77 (2008).
51 Team, R. C. (2017).
52 Pagel, M. & Meade, A. BayesTraits v. 2.0. *Reading: University of Reading* (2013).
53 Venditti, C., Meade, A. & Pagel, M. Multiple routes to mammalian diversity. *Nature* **479**, 393 (2011).
54 Adams, D. C. & Collyer, M. L. Multivariate phylogenetic comparative methods: evaluations, comparisons, and recommendations. *Systematic biology* **67**, 14-31 (2017).
55 Adams, D. C. & Felice, R. N. Assessing trait covariation and morphological integration on phylogenies using evolutionary covariance matrices. *PloS one* **9**, e94335 (2014).
56 Rohlf, F. J. & Corti, M. Use of two-block partial least-squares to study covariation in shape. *Systematic Biology*, 740-753 (2000).
57 Rohlf, F. J. & Slice, D. Extensions of the Procrustes method for the optimal superimposition of landmarks. *Systematic Biology* **39**, 40-59 (1990).
58 Bookstein, F. L. in *Advances in morphometrics* 131-151 (Springer, 1996).
59 Dryden, I. & Mardia, K. *Statistical analysis of shape*. (Wiley, 1998).
60 Siegel, A. F. & Benson, R. H. A robust comparison of biological shapes. *Biometrics*, 341-350 (1982).
61 Cardini, A. Integration and modularity in Procrustes shape data: is there a risk of spurious results? *Evolutionary Biology*, 1-16 (2018).
62 Chapman, R. E. in *Proceedings of the Michigan morphometrics workshop.* (University of Michigan Museum of Zoology, Ann Arbor).
63 Zelditch, M. L., Swiderski, D. L. & Sheets, H. D. *Geometric morphometrics for biologists: a primer*. (Academic Press, 2012).
64 Klingenberg, C. P. & McIntyre, G. S. Geometric morphometrics of developmental instability: analyzing patterns of fluctuating asymmetry with Procrustes methods. *Evolution* **52**, 1363-1375 (1998).
65 Bookstein, F. L. in *Image Fusion and Shape Variability Techniques.* 59-70 (Leeds: Leeds University Press).
66 Adams, D. C., Rohlf, F. J. & Slice, D. E. A field comes of age: geometric morphometrics in the 21st century. *Hystrix* **24**, 7 (2013).
67 Adams, D. C., Rohlf, F. J. & Slice, D. E. Geometric morphometrics: ten years of progress following the 'revolution'. *Italian Journal of Zoology* **71**, 5-16 (2004).
68 Adams, D. C., Collyer, M. L. & Kaliontzopoulou, A. (2018).
69 Zelditch, M. L., Ye, J., Mitchell, J. S. & Swiderski, D. L. Rare ecomorphological convergence on a complex adaptive landscape: body size and diet mediate evolution of jaw shape in squirrels (Sciuridae). *Evolution* **71**, 633-649 (2017).
70 Uyeda, J. C., Caetano, D. S. & Pennell, M. W. Comparative analysis of principal components can be misleading. *Systematic Biology* **64**, 677-689 (2015).
71 Chira, A. M. & Thomas, G. H. The impact of rate heterogeneity on inference of phylogenetic models of trait evolution. *Journal of evolutionary biology* **29**, 2502-2518 (2016).
72 Monteiro, L. R. Morphometrics and the comparative method: studying the evolution of biological shape. *Hystrix, the Italian Journal of Mammalogy* **24**, 25-32 (2013).
73 Adams, D. C. & Collyer, M. L. On the comparison of the strength of morphological integration across morphometric datasets. *Evolution* **70**, 2623-2631 (2016).
74 Mitteroecker, P. & Bookstein, F. The conceptual and statistical relationship between modularity and morphological integration. *Systematic biology* **56**, 818-836 (2007).

Figures legends:

Figure 1. How integration and selection direct phenotypic evolution. a) Approximate areas of simulated phenotypic evolution for high (dark grey ellipse) and zero (light grey circle) trait-covariation (modified from [13]). Higher integration entails exploration of more extreme trait values (following [17]); b) A complete modular organization between beak and skull shape (i.e. zero covariation) representing the extreme scenario of the condition proposed for the classic passerine adaptive radiations whereby the beak can evolve more freely [7,11,12]. This scenario permits the initial theoretical phenotype (small dark grey ellipse) reaching all three theoretical adaptive peaks (white ellipses), allowing greater evolutionary flexibility (e.g. [13,42]); c) The alternative scenario, an integrated organization between beak and skull shape (i.e. stronger covariation) strongly facilitates reaching the theoretical adaptive peak that is aligned with the axis of maximum phenotypic covariation (i.e. phenotypic line of least resistance, *sensu* [23]) to the detriment of the adaptive peaks that are not aligned with this axis [17,23,24]. Boundary lines are dashed to reflect that phenotypic evolution is more likely to happen within the area described by the covariation structure (yellow area) but can occur beyond those limits (greenish blue background), for instance if directional selection is strong enough (e.g. [43]).

Figure 2. Pattern and tempo of craniofacial evolution in landbirds. Phylomorphospaces of the first three principal components of shape (left), shape changes associated with these shape axes (centre), and rates of morphological evolution (right) for a) the whole skull; (b) 'beak'; and (c) 'skull' blocks. Light grey convex hull encloses Passeriformes, dark grey convex hull encloses Psittaciformes; purple dots represent Darwin's finches and pink dots represent Hawaiian honeycreepers (see Extended Data Figs 3-5 for the main landbird orders labelled in the phylomorphospaces). Branch colours in the phylogenies indicate relative rate of evolution. Inferred rate shifts with higher posterior probability than 0.7 are plotted in corresponding branches (circles) or nodes (triangles) in the phylogeny (see SI. Tables 1-3 for the full list of rate shifts). Posterior probability of each inferred rate shift is indicated by the size of said circle or triangle. Clade labels as in Figs. 3,4 and Table 1.

Figure 3. Evolutionary integration between the beak and the skull in landbirds. PLS1 plots for the Two Blocks-Phylogenetic Partial Least Squares Analyses using the rate-scaled phylogeny (situation 2, see Methods) in each clade (numbers correspond to clades as detailed in Table 1). Y axes show PLS1 scores beak block; X axes show PLS1 scores skull block. a) Major landbird lineages, b) major lineages of passerines. Purple dots represent Darwin's finches and pink dots represent Hawaiian honeycreepers.

Figure 4. Strength of cranial integration across landbirds and maximum phenotypic distances per family/subfamily. a) Z-scores and corresponding intervals of confidence for each major lineage of landbirds and (b) passerine parvorder. Z-scores are effect sizes from the randomized distribution of *rpls* values from the phylogenetic PLS for each clade (situation 2, two blocks, using the rate-scaled phylogeny; see Methods). Cladograms portray the simplified phylogenetic relationships of the main landbird lineages in our phylogeny (solid colours) as compared to other recently published phylogenetic hypothesis[29](transparent colour). (b) Brighter silhouettes represent the island passeroids Darwin's finches (purple) and Hawaiian honeycreepers (pink), whereas less contrasted silhouettes represent the island muscicapoids that radiated in Galapagos (greyish purple) and Hawaii (greyish pink). Our phylogeny is exactly coincident with Prum et al.'s[29] for the interrelationship of major passerine lineages. c) Maximum total Procrustes distances per family/subfamily for the 'beak' and the 'skull' blocks. d) Maximum PLS1 distances per family/subfamily for the 'beak' and 'skull' block. Labels in c and d correspond to families as detailed in Extended Data Fig. 9. Dot colours in c and d

607 correspond to the ages of the most common recent ancestor (MRCA) for each of the focal families in our MCC

608 tree.

609

610

611

612

613 ## Tables

614

615 **Table 1.** Pairwise comparisons of z-scores (strength of evolutionary covariation between beak and skull)
616 between clades and associated *P* values for situation 2 (two blocks, using the rate-scaled phylogeny, see
617 Methods). Bold values are statistically significant ($P < 0.05$). Each clade z-score value is provided. 1*Passerida
618 = Passerida excluding Darwin's finches and Hawaiian honeycreepers.

619

620

621

622

Z (means)	Clades	1	2	3	4	5	6	7	8	9	10	11	12	13
10.25	**1. All landbirds**													
5.47	**2. Non-Passerines**	***0.0196***												
7.62	**3. Passeriformes**	0.4057	***0.0245***											
5.63	**4. Passeri**	0.2287	0.1715	0.1986										
2.71	**5. Tyranni**	0.0943	0.4649	0.0847	0.2324									
5.03	**6. Psittaciformes**	0.2087	***0.0250***	0.2683	0.1147	0.0532								
0.24	**7. Falconiformes**	***0.0016***	***0.0301***	***0.0017***	***0.0091***	0.0642	***0.0015***							
0.80	**8. Piciformes**	***0.0003***	***0.0237***	***0.0005***	***0.0052***	0.0720	***0.0008***	0.3873						
0.76	**9. Coraciiformes**	***0.0033***	0.0584	***0.0034***	***0.0182***	0.1103	***0.0031***	0.3675	0.4652					
1.38	**10. Bucerotiformes**	***0.0183***	0.1643	***0.0172***	0.0642	0.2292	***0.0125***	0.2224	0.2814	0.3272				
1.36	**11. Trogoniformes**	***0.0083***	0.1189	***0.0083***	***0.0402***	0.1885	***0.0069***	0.2420	0.3087	0.3564	0.4609			
1.21	**12. Eucavitaves**	***0.0001***	***0.0165***	***0.0001***	***0.0029***	0.0719	***0.0004***	0.3380	0.4453	0.4898	0.3074	0.3389		
1.26	**13. Strigiformes**	***0.0071***	0.1066	***0.0071***	***0.0354***	0.1740	***0.0061***	0.2598	0.3318	0.3781	0.4391	0.4769	0.3648	
0.83	**14. Accipitriformes**	***0.0008***	***0.0345***	***0.0010***	***0.0086***	0.0865	***0.0013***	0.3716	0.4775	0.4862	0.3038	0.3326	0.4718	0.3556

Main passerine lineages

Z (means)	Clades	1	1*	2	3	4	5	6
4.22	**P1.Passerida**							
2.95	**P1*.Passerida***	0.2589						
-0.92	**P2. Muscicapida**	***0.0004***	***0.0042***					
1.01	**P3. Sylviida**	***0.0310***	0.1133	0.0853				
1.48	**P4. Corvides**	***0.0344***	0.1352	***0.0483***	0.4225			
1.66	**P5. Meliphagoidea**	0.1284	0.2916	***0.0321***	0.2881	0.3401		
1.33	**P6. Tyrannida**	0.0635	0.1838	0.0544	0.3956	0.4631	0.3831	
0.00	**P7. Furnariida**	***0.0053***	***0.0287***	0.2609	0.2431	0.1755	0.1143	0.1739

623

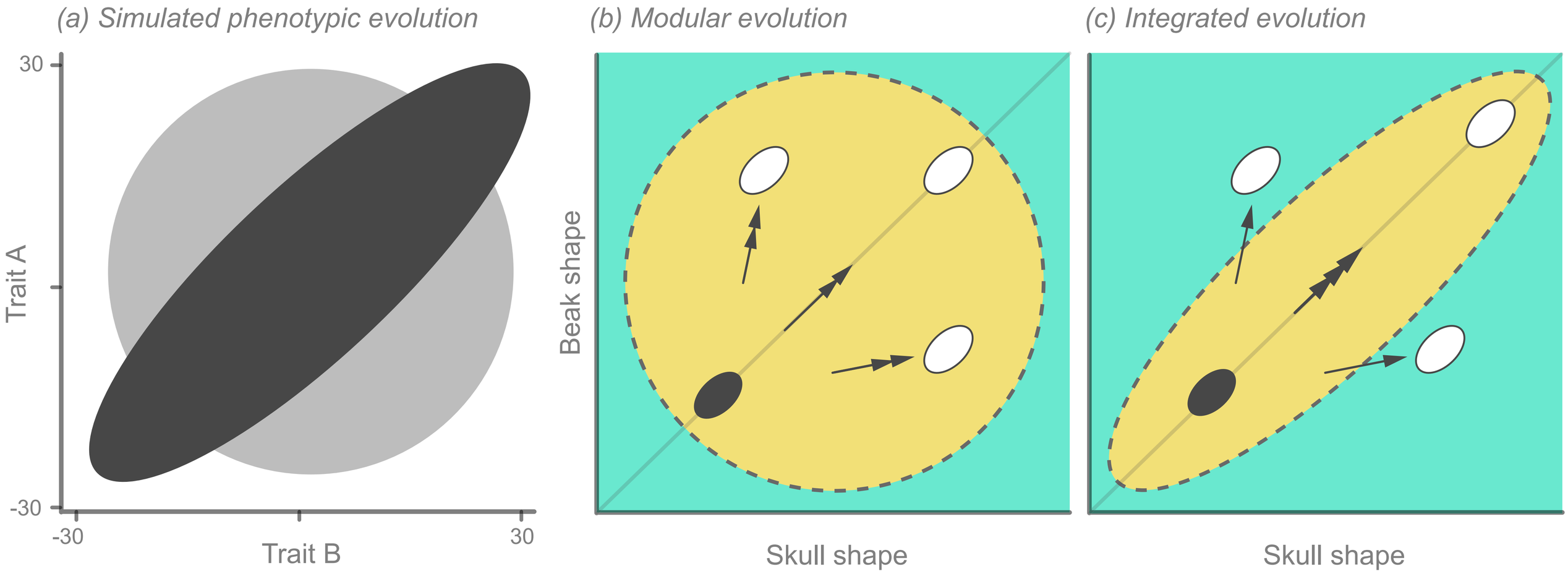
(a) Simulated phenotypic evolution
30
-30
Trait A
-30
30
Trait B
(b) Modular evolution
Beak shape
Skull shape
(c) Integrated evolution
Skull shape

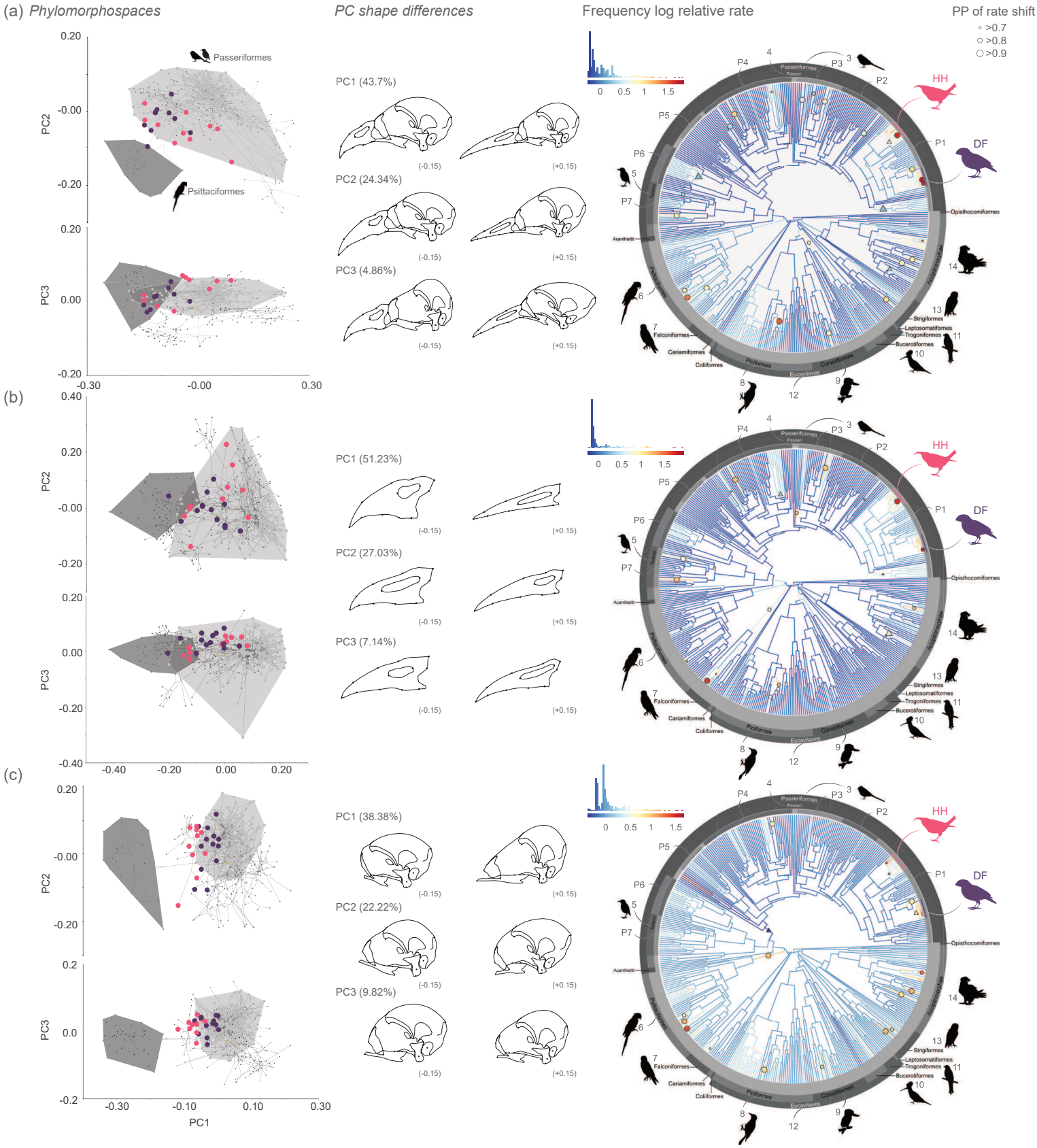
(a) Phylomorphospaces
PC shape differences
Frequency log relative rate
PP of rate shift
>0.7
>0.8
>0.9
Passeriformes
Psittaciformes
PC1 (43.7%)
PC2 (24.34%)
PC3 (4.86%)
(b)
PC1 (51.23%)
PC2 (27.03%)
PC3 (7.14%)
(c)
PC1 (38.38%)
PC2 (22.22%)
PC3 (9.82%)
HH
DF
Opisthocomiformes
Strigiformes
Leptosomatiformes
Trogoniformes
Bucerotiformes
Falconiformes
Cariamiformes
Coliiformes
Piciformes
Coraciiformes
Eucavitaves
PC1
PC2
PC3

(a) *Phylogenetic Partial Least Squares*

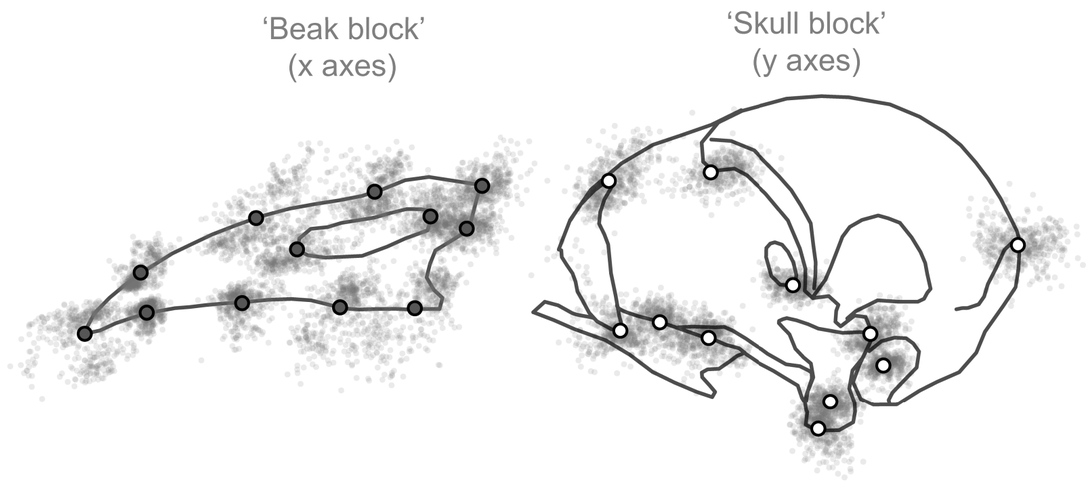

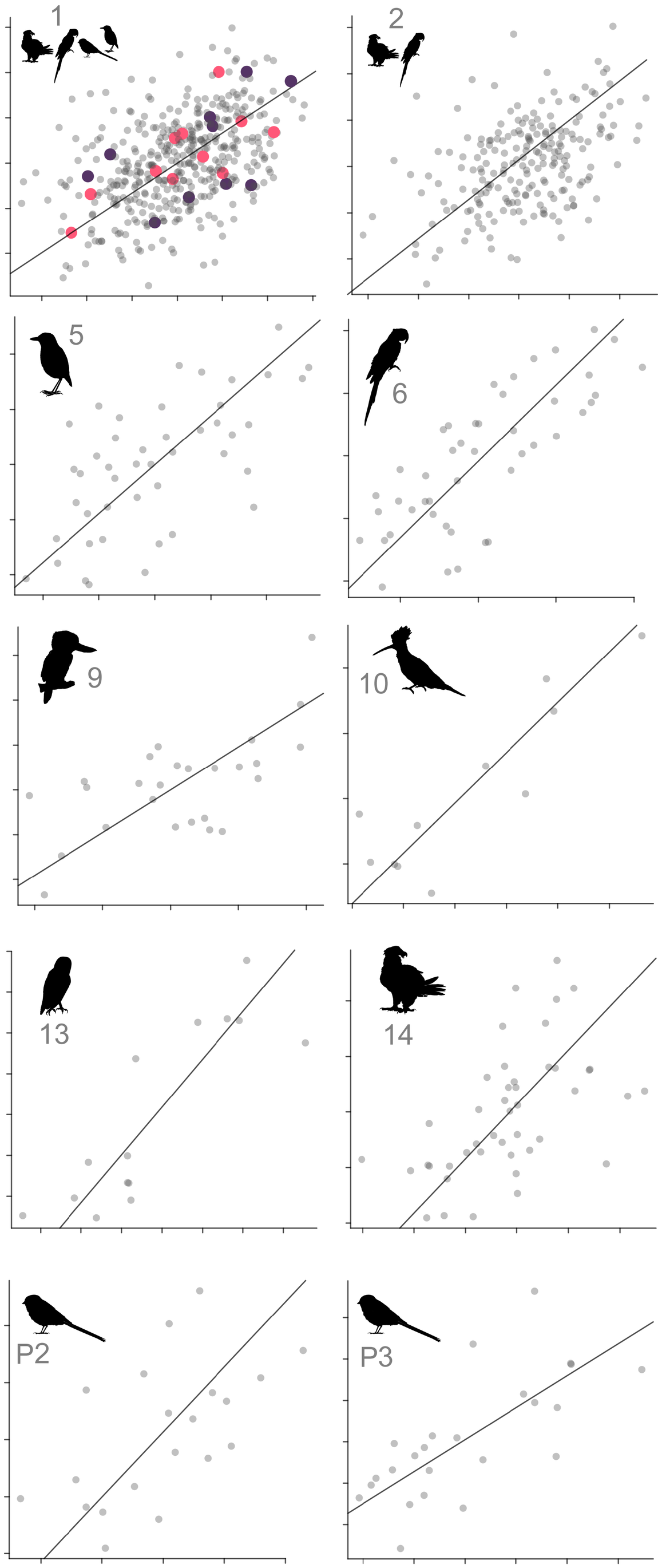

(b)

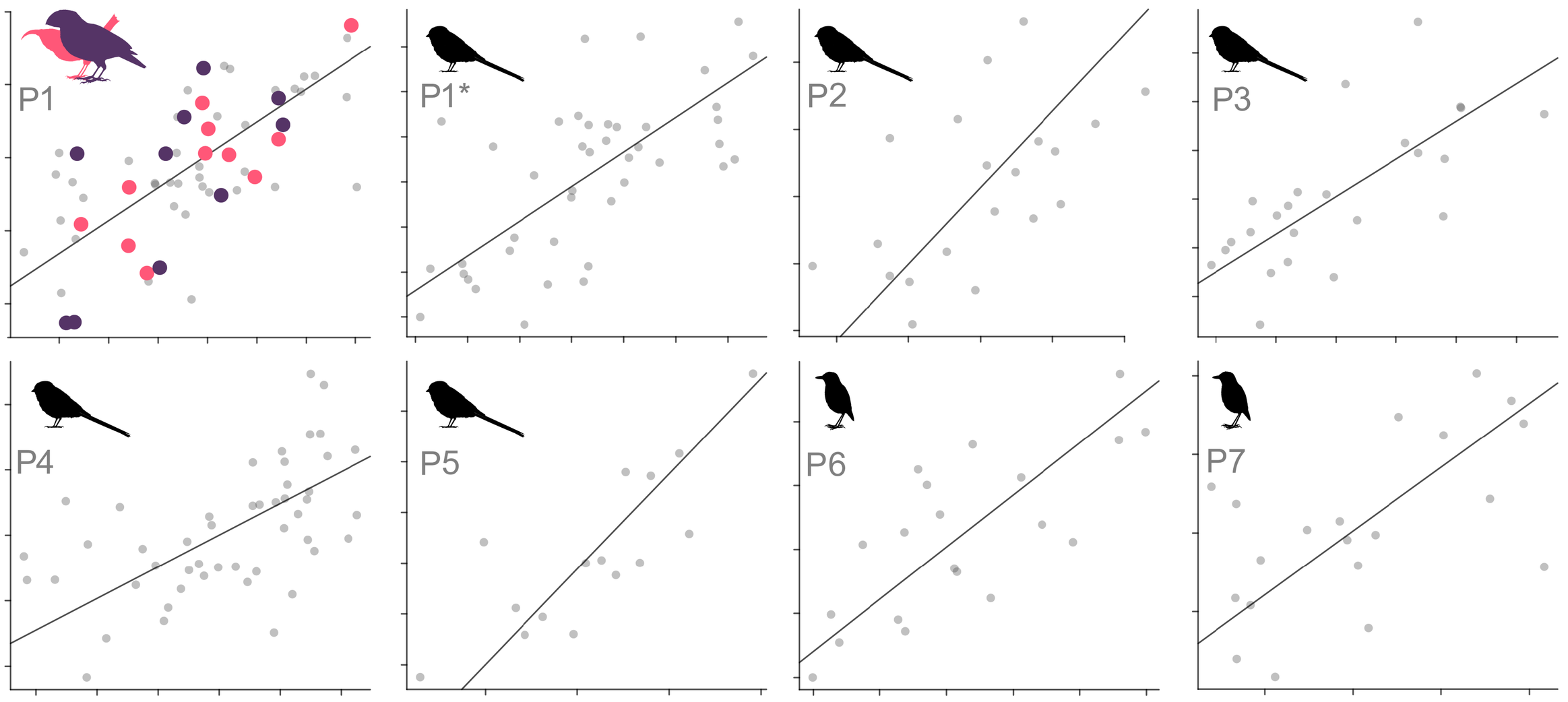

(a) *Levels of integration*

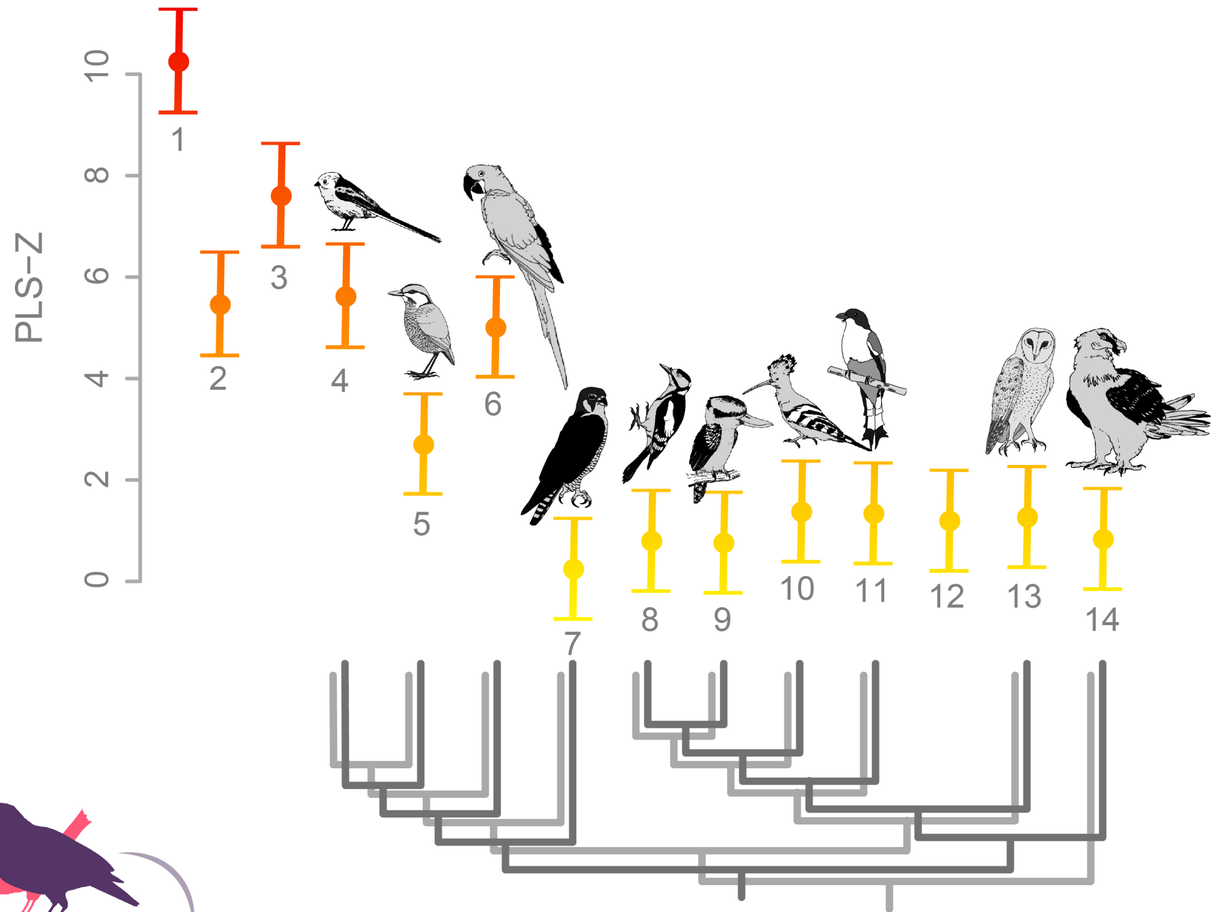

(b)

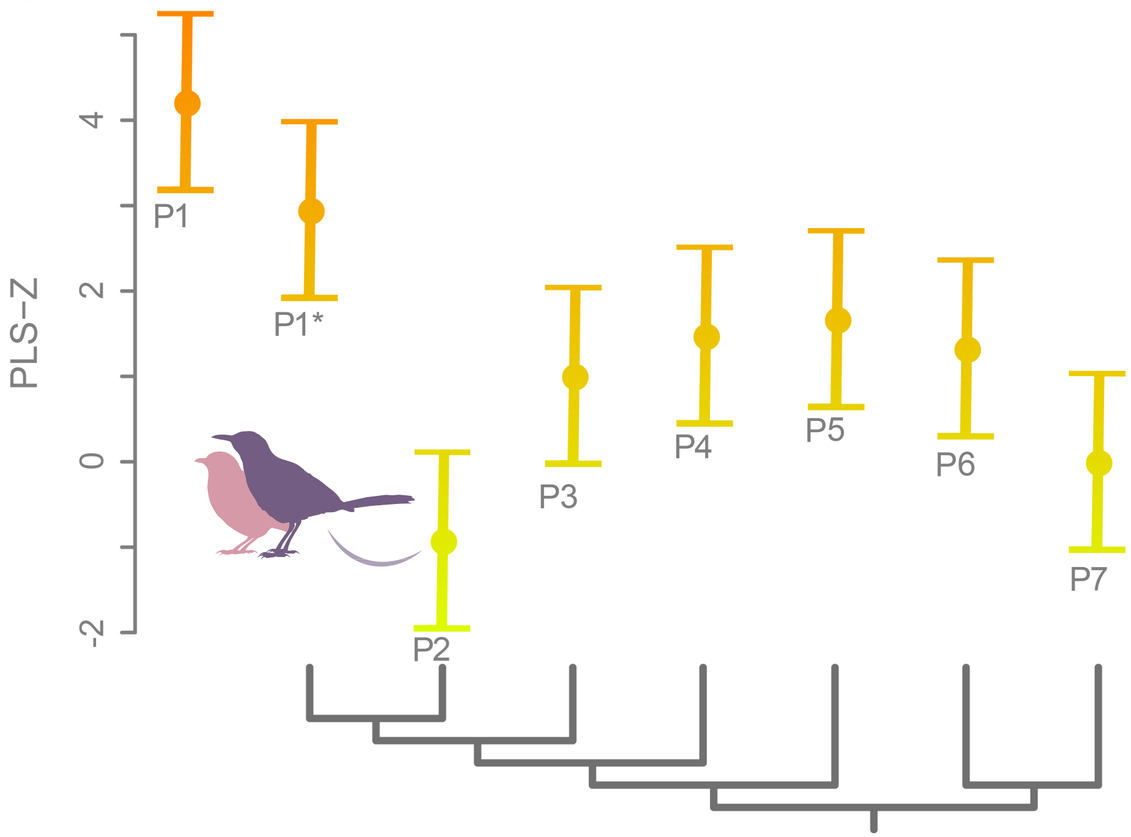

(c) *Max. Proc. Distance within family*

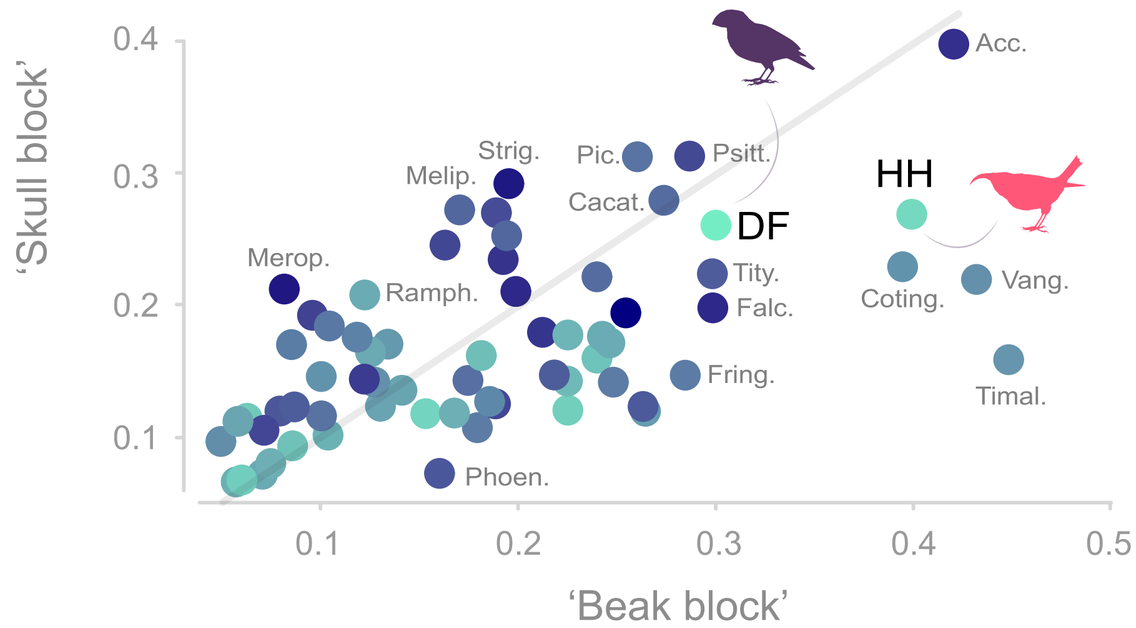

MRCA Age (MY) 40 30 20 10

(d) *Max. PLS1 Distance within family*

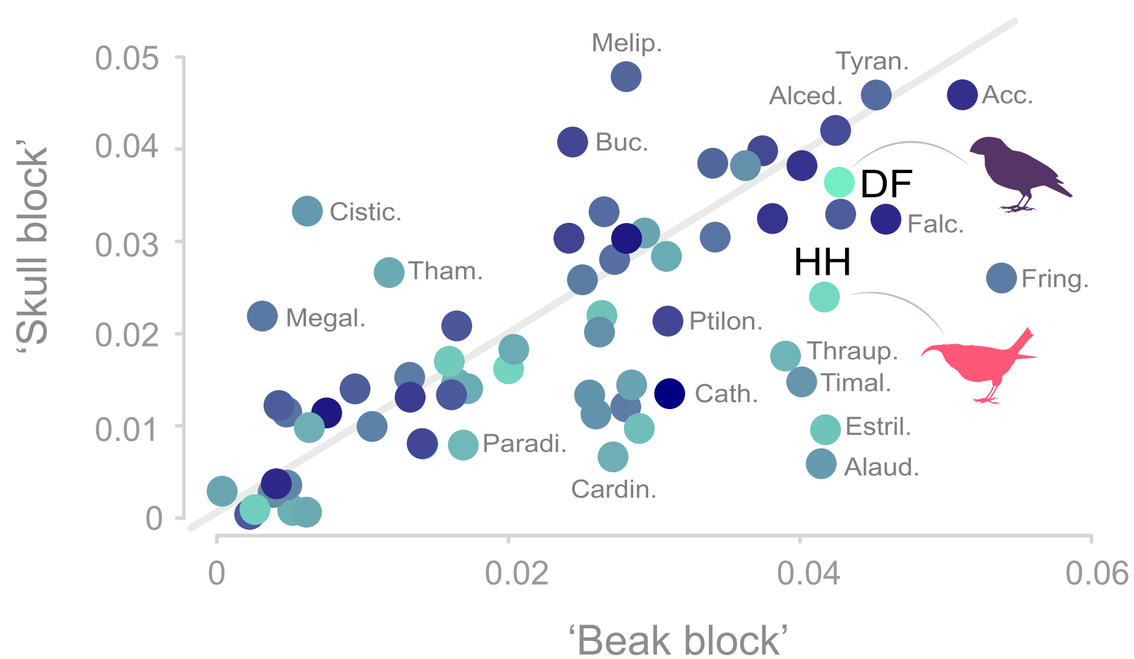

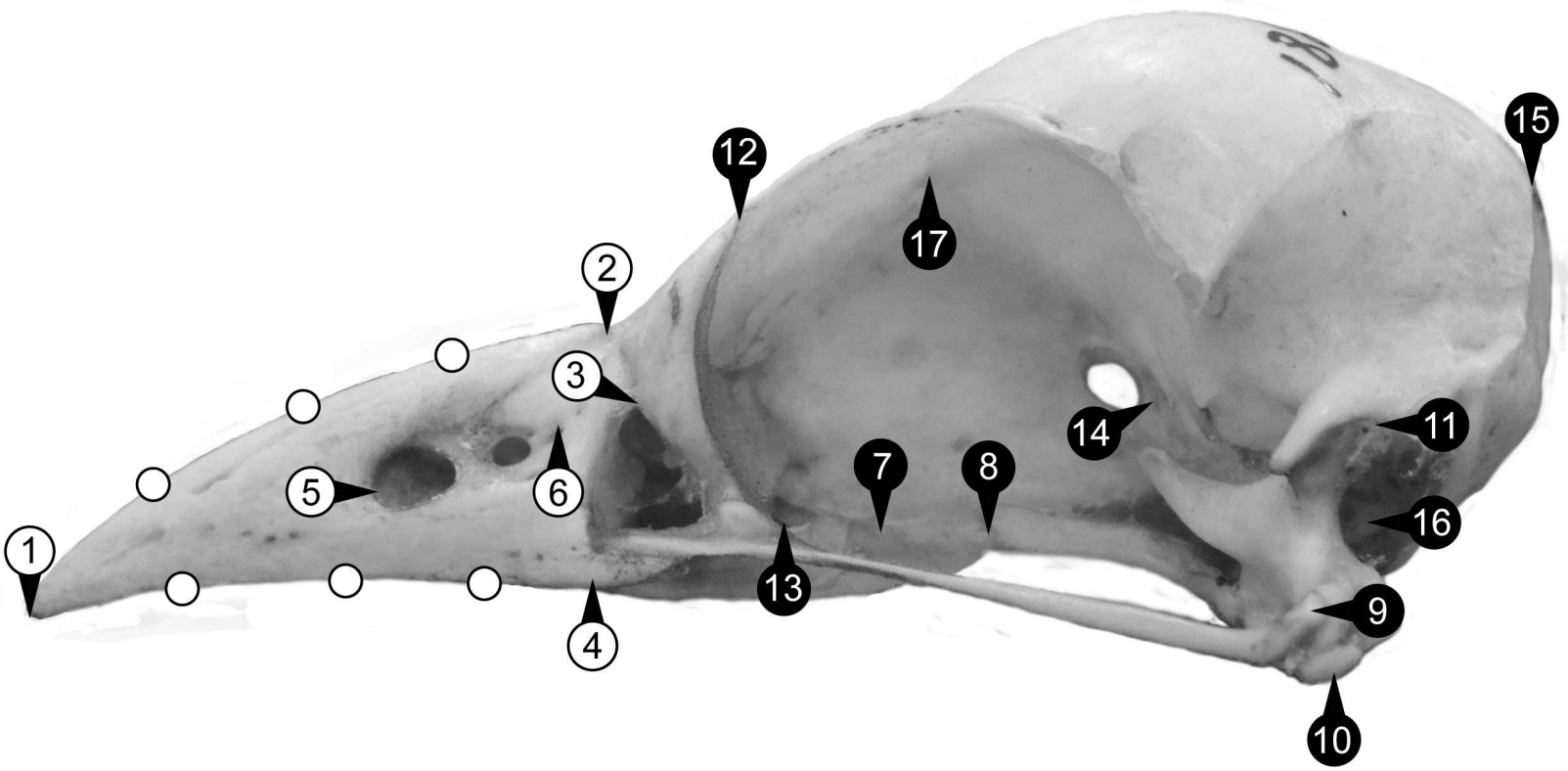
1
2
3
4
5
6
7
8
9
10
11
12
13
14
15
16
17

N	Block	Anatomical region	Description
1	Beak	Rostrum	Anterior tip of the premaxillary symphysis
2	Beak	Rostrum	Nasofrontal hinge
3	Beak	Rostrum	Ventrolateral end of the contact between nasal and lacrimal (or lacrimal-ectethmoid complex**)
4	Beak	Rostrum	Anteriormost edge of antorbital fossa orthogonally projected to the ventral rim of the maxilla
5	Beak	Rostrum	Anteriormost point of external naris fossa
6	Beak	Rostrum	Posteriormost point of external naris fossa
7	Skull	Palate	Middle point of the medial contact between palatines
8	Skull	Palate	Middle point of the lateral contact of palatine and pterygoid
9	Skull	Quadrate	Medial condyle of quadrate
10	Skull	Quadrate	Contact of jugal bar and quadrate
11	Skull	Quadrate	Lateral contact of ootic process of quadrate and squamosal
12	Skull	Lacrimal-ectethmoid	Posterolateral tip of lacrimal (or lacrimal-ectethmoid complex**)
13	Skull	Lacrimal-ectethmoid	Posterolateral end of the contact between lacrimal (or lacrimal-ectethmoid complex**) and frontal
14	Skull	Neurocranium	Ventralmost point of the foramen of the optic nerve
15	Skull	Neurocranium	Intersection of *crista nuchalis transversus* and *crista nuchalis sagittalis*
16	Skull	Neurocranium	External ear (geometric centre of the auditory meatus)
17	Skull	Neurocranium	Foramen of the olfactory nerve (geometric centre)
18-21	Beak	Rostrum	Curve 1 of three semilandmarks along the beak culmen
21-24	Beak	Rostrum	Curve 2 of three semilandmarks along the right tomial ridge
			** term coined by Cracraft[1] to describe the coordinated evolution of both bones in modern birds which we used for the purposes of landmarking.

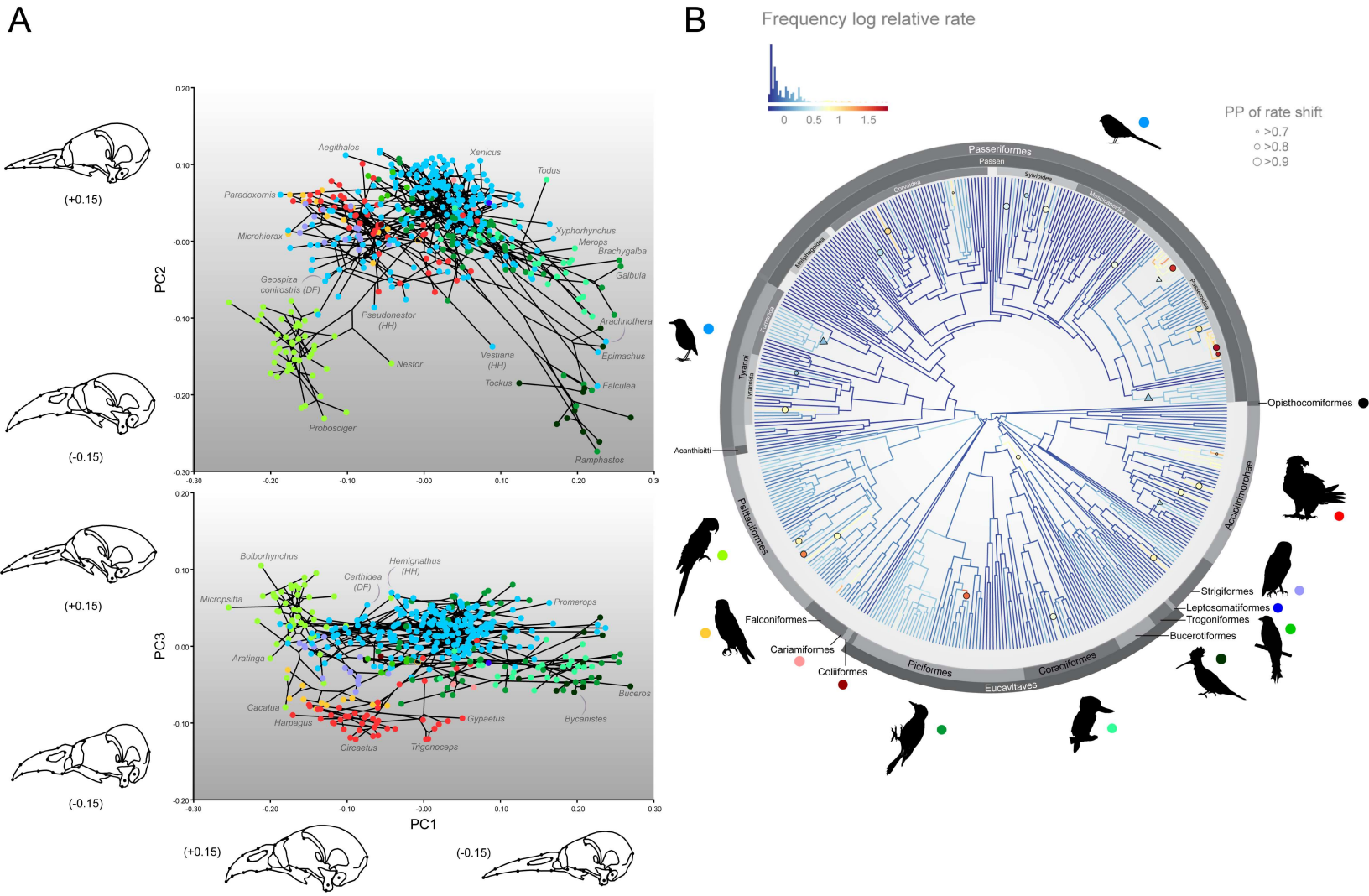
A
B
Frequency log relative rate
0
0.5
1
1.5
PP of rate shift
>0.7
>0.8
>0.9
PC2
PC3
PC1
(+0.15)
(-0.15)
Aegithalos
Xenicus
Todus
Paradoxornis
Xyphorhynchus
Microhierax
Meropa
Brachygalba
Galbula
Geospiza conirostris (DF)
Pseudonestor (HH)
Arachnothera
Epimachus
Vestiaria (HH)
Nestor
Tockus
Falculea
Prosobsiger
Ramphastos
Bolborhynchus
Hemignathus (HH)
Certhidea (DF)
Micropsitta
Promerops
Aratinga
Cacatua
Harpagus
Gypaetus
Bycanistes
Buceros
Circaetus
Trigonoceps
Passeriformes
Passeri
Sylvioidea
Corvoidea
Meliphagoidea
Passerida
Tyranni
Tyrannida
Acanthisitti
Opisthocomiformes
Acipitrimorphae
Psittaciformes
Strigiformes
Leptosomatiformes
Trogoniformes
Bucerotiformes
Falconiformes
Cariamiformes
Coliiformes
Piciformes
Coraciiformes
Eucavitaves

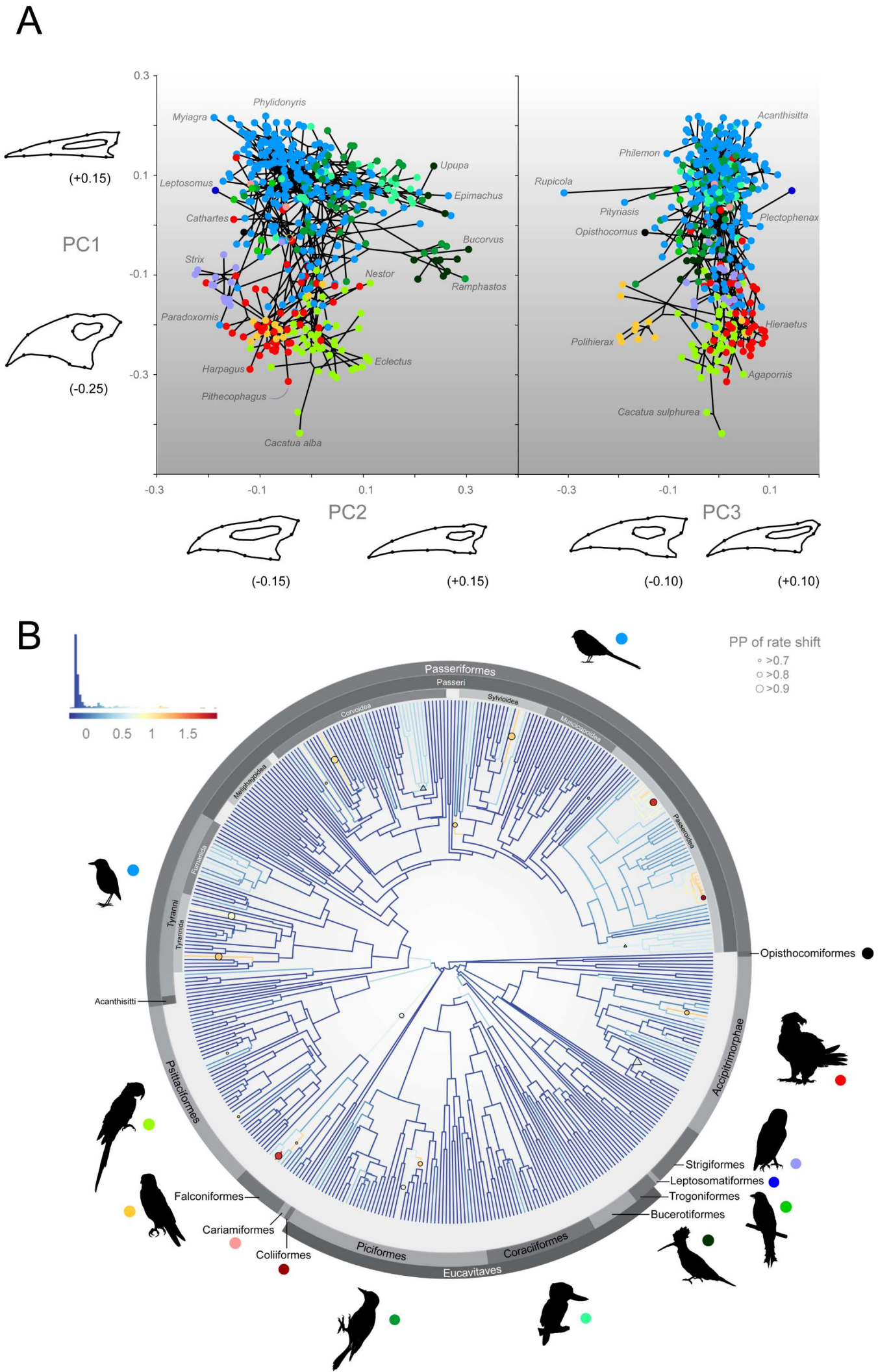
A
PC1
PC2
PC3
(+0.15)
(-0.25)
(-0.15)
(+0.15)
(-0.10)
(+0.10)
Phylidonyris
Myiagra
Upupa
Leptosomus
Epimachus
Cathartes
Bucorvus
Strix
Nestor
Ramphastos
Paradoxornis
Eclectus
Harpagus
Pithecophagus
Cacatua alba
Acanthisitta
Philemon
Rupicola
Pityriasis
Plectophenax
Opisthocomus
Hieraetus
Polihierax
Agapornis
Cacatua sulphurea
B
PP of rate shift
>0.7
>0.8
>0.9
0
0.5
1
1.5
Passeriformes
Passeri
Corvoidea
Sylvioidea
Muscicapoidea
Meliphagoidea
Passeroidea
Eurylaimida
Tyranni
Tyrannida
Acanthisitti
Psittaciformes
Falconiformes
Cariamiformes
Coliiformes
Piciformes
Coraciiformes
Eucavitaves
Accipitrimorphae
Opisthocomiformes
Strigiformes
Leptosomatiformes
Trogoniformes
Bucerotiformes

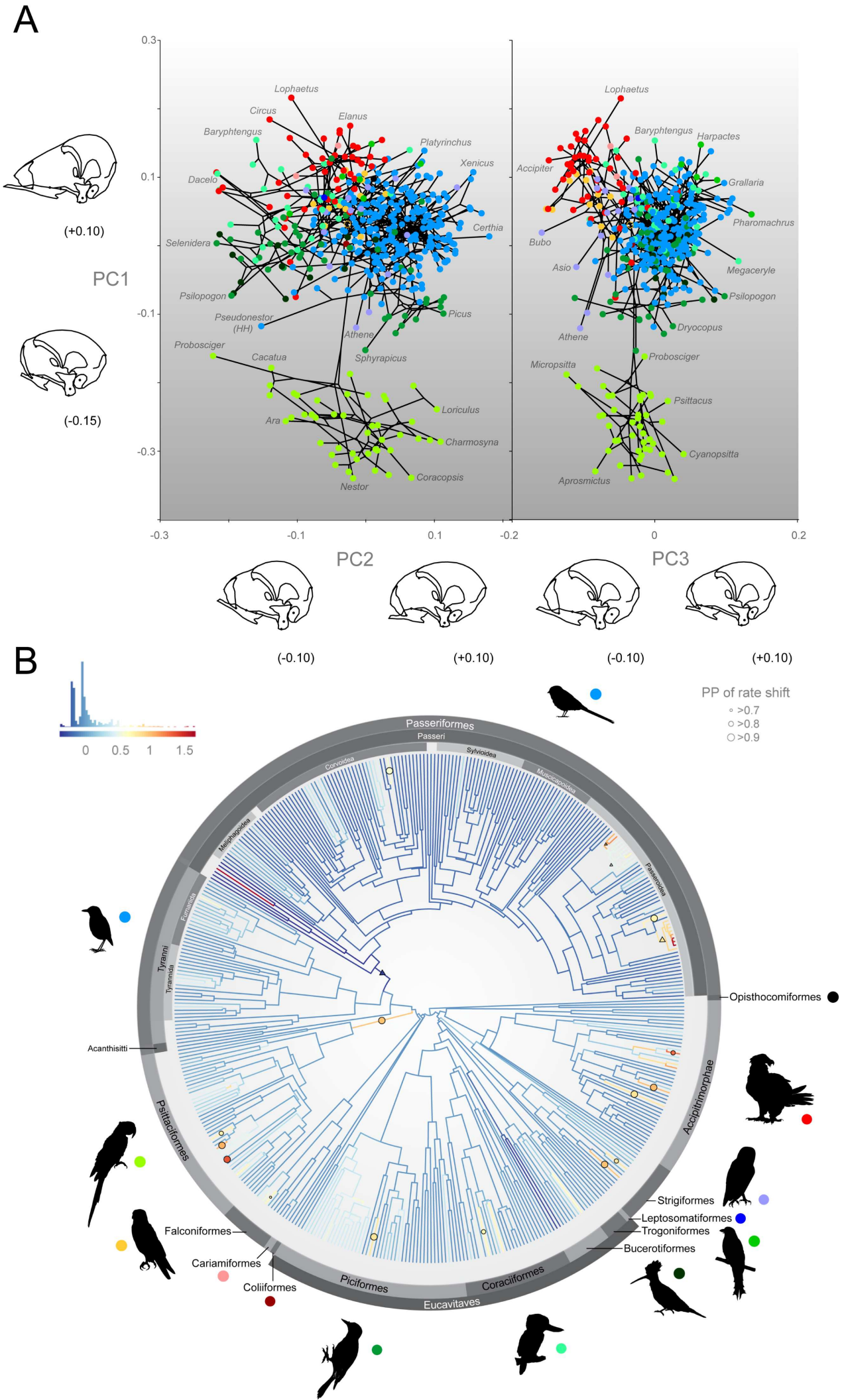
A
0.3
0.1
-0.1
-0.3
PC1
(+0.10)
(-0.15)
Lophaetus
Circus
Elanus
Baryphtengus
Platyrinchus
Xenicus
Dacelo
Certhia
Selenidera
Psilopogon
Pseudonestor (HH)
Picus
Athene
Sphyrapicus
Probosciger
Cacatua
Loriculus
Ara
Charmosyna
Coracopsis
Nestor
Lophaetus
Baryphtengus
Harpactes
Accipiter
Grallaria
Pharomachrus
Bubo
Asio
Megaceryle
Psilopogon
Dryocopus
Athene
Probosciger
Micropsitta
Psittacus
Cyanopsitta
Aprosmictus
-0.3
-0.1
0.1
-0.2
0
0.2
PC2
PC3
(-0.10)
(+0.10)
(-0.10)
(+0.10)
B
0
0.5
1
1.5
PP of rate shift
>0.7
>0.8
>0.9
Passeriformes
Passeri
Sylvioidea
Muscicapoidea
Passeroidea
Meliphagoidea
Corvoidea
Furnariida
Tyranni
Tyrannida
Acanthisitti
Psittaciformes
Accipitrimorphae
Opisthocomiformes
Strigiformes
Leptosomatiformes
Trogoniformes
Bucerotiformes
Coraciiformes
Eucavitaves
Piciformes
Coliiformes
Cariamiformes
Falconiformes

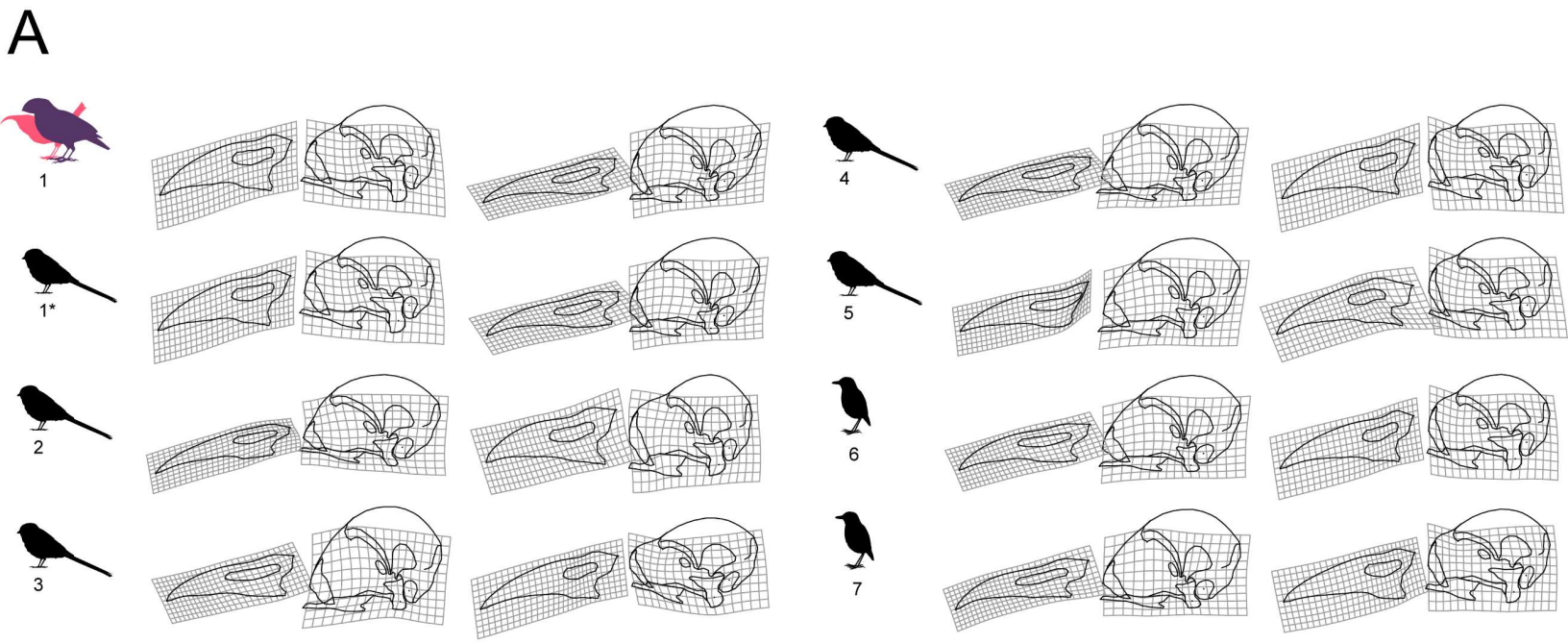
A
1
1*
2
3
4
5
6
7

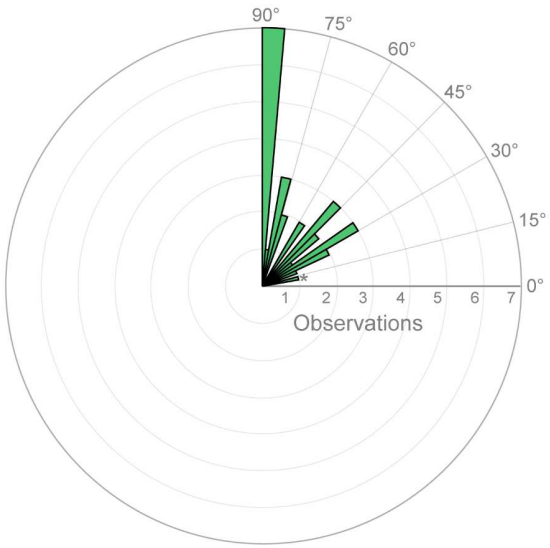
B
90°
75°
60°
45°
30°
15°
0°
1
2
3
4
5
6
7
Observations

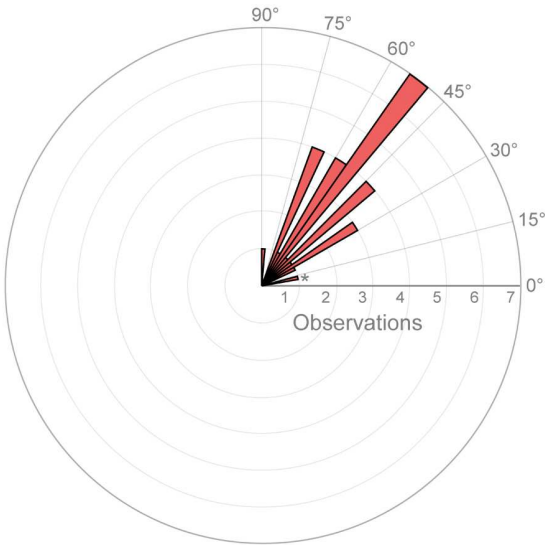
C
90°
75°
60°
45°
30°
15°
0°
1
2
3
4
5
6
7
Observations

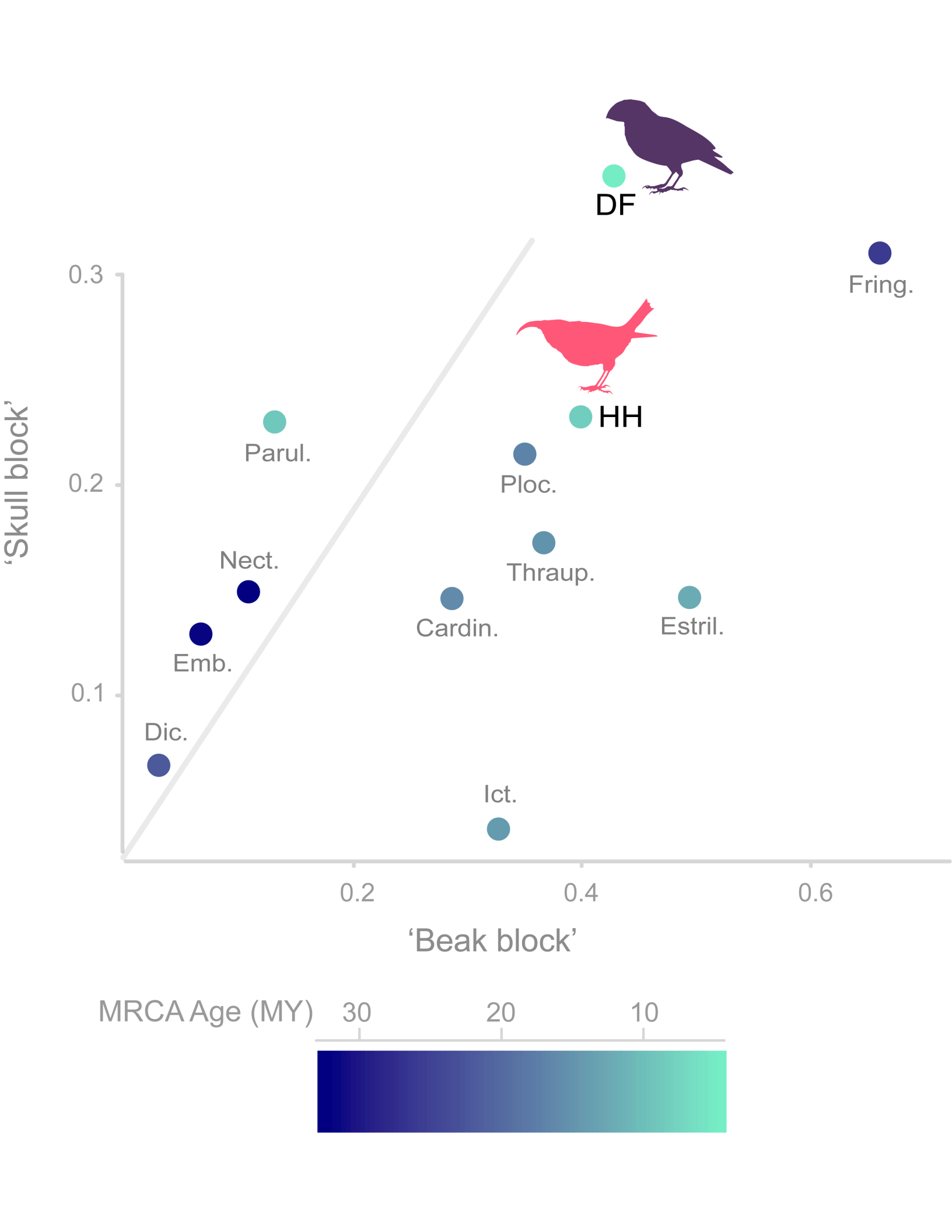
DF
Fring.
HH
Parul.
Ploc.
Nect.
Thraup.
Cardin.
Estril.
Emb.
Dic.
Ict.
0.3
0.2
0.1
0.2
0.4
0.6
'Skull block'
'Beak block'
MRCA Age (MY)
30
20
10

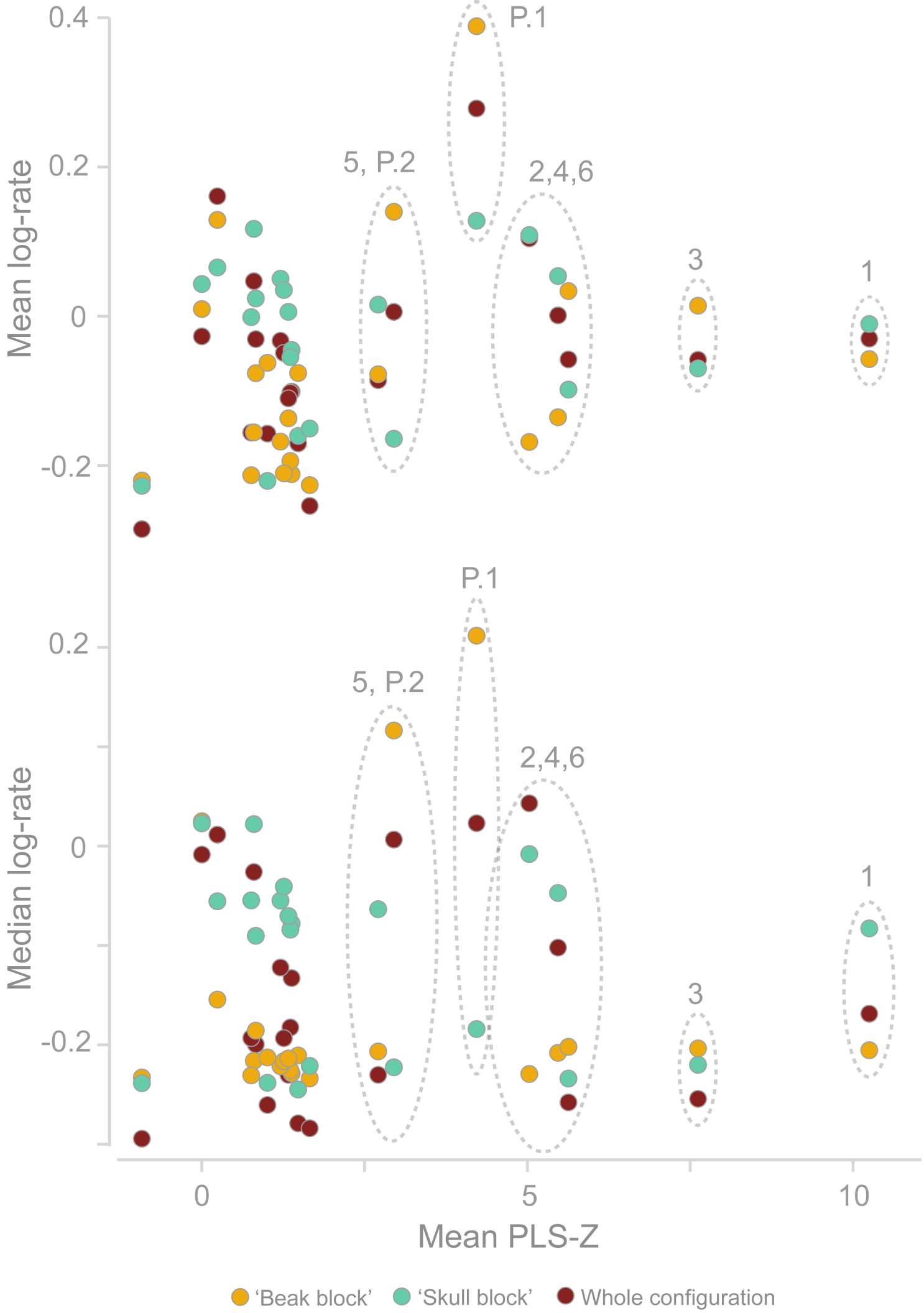
0.4
0.2
0
-0.2
Mean log-rate
P.1
5, P.2
2,4,6
3
1
0.2
0
-0.2
Median log-rate
P.1
5, P.2
2,4,6
3
1
0
5
10
Mean PLS-Z
'Beak block'
'Skull block'
Whole configuration

Label	Family
Acanth.	Acanthisittidae
Acc.	Accipitridae
Alaud.	Alaudidae
Alced.	Alcedinidae
Brachyp.	Brachypteraciidae
Buc.	Bucerotidae
Bucc.	Bucconidae
Cacat.	Cacatuidae
Cardin.	Cardinalidae
Cath.	Cathartidae
Cistic.	Cisticolidae
Corac.	Coraciidae
Corv.	Corvidae
Coting.	Cotingidae
Crac.	Cracticidae
DF	Darwin's finches (Geospizinae, Thraupidae)
Dic.	Dicaedidae
Ember.	Emberizidae
Estril.	Estrildidae
Euryl.	Eurylaimidae
Falc.	Falconidae
Fring.	Fringillidae (excluding Hawaiian honeycreepers)
Furn.	Furnariidae
Galb.	Galbulidae
HH	Hawaiian honeycreepers (Drepanidinae, Fringillidae)
Hirun.	Hirundinidae
Ict.	Icteridae
Lyb.	Lybiidae
Megal.	Megalaimidae
Melip.	Meliphagidae
Merop.	Meropidae
Momot.	Momotidae
Nect.	Nectariniidae
Paradi.	Paradisaeidae
Parul.	Parulidae
Phoen.	Phoeniculidae
Pic.	Picidae
Pipr.	Pipridae
Pitt.	Pittidae
Ploc.	Ploceidae
Psitt.	Psittacidae
Ptilon.	Ptilonorhynchidae
Ramph.	Ramphastidae
Strig.	Strigidae
Sturn.	Sturnidae
Sylv.	Sylviidae
Tham.	Thamnophilidae
Thraup.	Thraupidae (excluding Darwin's finches)
Timal.	Timaliidae
Tity.	Tityridae
Trog.	Trogonidae
Tyran.	Tyrannidae
Vang.	Vangidae

ϴ			
BEAK	**Passeriformes**	**Passeri**	**Tyranni**
Passeroidea	27.57	23.17	44.37
Passeroidea*	31.35	28.70	43.59
Muscicapoidea	71.24	70.33	82.03
SKULL			
Passeroidea	30.98	27.51	41.32
Passeroidea*	33.69	29.63	43.42
Muscicapoidea	56.16	58.51	60.18